IMPLEMENTATION OF DIRECTION FINDING WITH FREQUENCY DIVERSE ARRAY

A THESIS SUBMITTED TO
THE GRADUATE SCHOOL OF NATURAL AND APPLIED SCIENCES
OF
MIDDLE EAST TECHNICAL UNIVERSITY

BY

ARSEN TURHANER

IN PARTIAL FULFILLMENT OF THE REQUIREMENTS
FOR
THE DEGREE OF MASTER OF SCIENCE
IN
ELECTRICAL AND ELECTRONICS ENGINEERING

JULY 2017

Approval of the thesis:

IMPLEMENTATION OF DIRECTION FINDING WITH FREQUENCY DIVERSE ARRAY

submitted by **ARSEN TURHANER** in partial fulfillment of the requirements for the degree of **Master of Science in Electrical and Electronics Engineering Department, Middle East Technical University** by,

Prof. Dr. Gülbin Dural _____
Dean, Graduate School of **Natural and Applied Sciences**

Prof. Dr. Tolga Çiloğlu _____
Head of Department, **Electrical and Electronics Engineering**

Prof. Dr. Şimşek Demir _____
Supervisor, **Electrical and Electronics Eng. Dept., METU**

Examining Committee Members:

Prof. Dr. Sencer Koç
Electrical and Electronics Eng. Dept., METU _____

Prof. Dr. Şimşek Demir
Electrical and Electronics Eng. Dept., METU _____

Prof. Dr. Mustafa Kuzuoğlu
Electrical and Electronics Eng. Dept., METU _____

Prof. Dr. Ali Özgür Yılmaz
Electrical and Electronics Eng. Dept., METU _____

Doc. Dr. Asım Egemen Yılmaz
Electrical and Electronics Eng. Dept., Ankara University _____

Date: _____

I hereby declare that all information in this document has been obtained and presented in accordance with academic rules and ethical conduct. I also declare that, as required by these rules and conduct, I have fully cited and referenced all material and results that are not original to this work.

Name, Last Name: ARSEN TURHANER

Signature :

ABSTRACT

IMPLEMENTATION OF DIRECTION FINDING WITH FREQUENCY DIVERSE ARRAY

Turhaner, Arsen

M.S., Department of Electrical and Electronics Engineering

Supervisor : Prof. Dr. Şimşek Demir

July 2017, 75 pages

Frequency Diverse Array (FDA) is a recent concept with lots of advantages that are emerged for the radar applications. In order to implement FDA practically, Linear Frequency Modulation (LFM) based FDA is recently offered. A tunable oscillator with delay lines is enough for the implementation. This novel design caught up the gaps of the FDA for a cheap implementation.

In order to implement radar, there should be lots of features in the signal processing as well as in the RF front-end. One of the important features of radar is the direction finding (DF). In this thesis, various methods for the implementation of DF for LFM based FDA radar are proposed.

In the flow of the thesis, theories behind the FDA and LFM based FDA are reviewed. Two methods for the implementation of the DF for LFM based FDA are suggested and demonstrated with the experiments. Results, possible improvements and future studies are shared with the reader.

Keywords: LFM based FDA, monopulse direction finding, FDA, null tracking

ÖZ

AYRIK FREKANSLI DİZİLERDE YÖN TAYİNİ UYGULAMASI

Turhaner, Arsen
Yüksek Lisans, Elektrik ve Elektronik Mühendisliği Bölümü
Tez Yöneticisi : Prof. Dr. Şimşek Demir

Temmuz 2017 , 75 sayfa

Ayrık Frekanslı Diziler (AFD), radar uygulamaları için birçok avantaja sahip olduğu ortaya çıkmış yeni bir kavramdır. Yakın geçmişte, AFD'yi pratik bir şekilde uygulayabilmek için, Doğrusal Frekans Kiplemeli (LFM) AFD önerilmiştir. Uygulama için geciktirme elemanlarına sahip frekansı ayarlanabilir bir osilatör yeterlidir. Bu yeni tasarım, düşük maliyetli bir uygulama yaratabilmek için AFD'nin boşluklarını kapatmış durumdadır.

Bir radar için, RF ön uçta olduğu kadar sinyal işlemede de çok sayıda özellik bulunmalıdır. Radarın önemli özelliklerinden birisi de yön bulmadır. Bu tezde, LFM tabanlı AFD radarı için yön bulma uygulaması olarak çeşitli yöntemler önerilmiştir.

Tezin akışında, AFD ve LFM tabanlı AFD'nin teorileri gözden geçirilmiştir. LFM tabanlı AFD'de yön bulma uygulaması için iki yöntem öne sürülmüş ve deneylerle sunulmuştur. Sonuçlar, muhtemel geliştirmeleri ve gelecekteki muhtemel çalışmalarıyla birlikte okuyucu ile paylaşılmıştır.

Anahtar Kelimeler: doğrusal frekans kiplemeli ayrık frekanslı diziler, tek darbeli yön bulma, ayrık frekanslı diziler, hüzme sıfırı takibi

To my family

ACKNOWLEDGMENTS

First of all, I am grateful to my family for their endless support throughout all my education.

I am also grateful to Simsek DEMİR and Altunkan HIZAL who are the owners and developers of the original idea about this study.

I want to thank Taylan EKER for his support to this study. I used his setup for my experiments which was in excellent condition.

I want to thank Çağrı ÇETİNTEPE for his great contributions. I couldn't get familiar with the setup without his instructions. Also I used his application in the experiments which includes SCPI commands to control instruments. This application dramatically reduced the durations of the experiments.

I also want to convey my special thanks to Savaş KARADAĞ and Enis KOBAL for their help during this study.

TABLE OF CONTENTS

ABSTRACT v

ÖZ vi

ACKNOWLEDGMENTS viii

TABLE OF CONTENTS ix

LIST OF TABLES xiii

LIST OF FIGURES xiv

LIST OF ABBREVIATIONS xvii

CHAPTERS

1 INTRODUCTION 1

2 FREQUENCY SCANNING RADAR AND FREQUENCY DIVERSE ARRAY IN LITERATURE AND MOTIVATION 5

2.1 Frequency Scanning Radar 5

2.1.1 Brief Review of Frequency Scanning Radar 5

2.1.2 Monopulse Direction Finding for Frequency Scanning Radar 6

2.2 Frequency Diverse Array 7

2.2.1 Brief Review of Frequency Diverse Array 7

2.2.2 Range-angle Coupling of Frequency Diverse Array 10

2.3 Summary of the Study 10

2.4 Organization of the Thesis 11

3 LINEAR FREQUENCY MODULATION BASED FREQUENCY DIVERSE ARRAY ANALYSIS AND DIRECTION FINDING METHODS 13

3.1 Linear Frequency Modulation based Frequency Diverse Array Analysis 13

3.1.1 Setup of the Array 13

3.1.2 Mathematical Derivations 14

3.2 Monopulse Direction Finding Methods for Linear Frequency Modulation based Frequency Diverse Array and Possible Improvements 16

3.2.1 Method 1: Using Time Data 18

3.2.2 Method 2: Using Frequency Content of the Received Signal 23

3.2.3 Comparison of the Methods 25

3.2.4 Possible Improvements 26

3.2.4.1 Pattern Recognition 26

3.2.4.2 Using Low Sidelobe Antenna Pattern . 28

3.2.4.3 Digital Beam Forming 29

3.2.4.4 Focusing on a Specific Angular Sector 30

4 DIRECTION FINDING EXPERIMENTS FOR LINEAR FREQUENCY MODULATION BASED FREQUENCY DIVERSE ARRAY 31

4.1 Experimental Setup 32

4.1.1 Encountered Difficulties in the Implementation Phase 39

4.2 Results of the Experiments 43

4.2.1 Results of the First Experiment 43

4.2.1.1 Scenario 1 43

4.2.1.2 Scenario 2 45

4.2.1.3 Scenario 3 46

4.2.1.4 Scenario 4 47

4.2.2 Results of the Second Experiment 48

4.2.2.1 Scenario 1 48

4.2.2.2 Scenario 2 50

4.2.2.3 Scenario 3 51

4.2.2.4 Scenario 4 53

4.2.2.5 Summary of the Second Experiment . 55

4.2.3 Results of the Third Experiment 56

4.2.3.1 Scenario 1 56

4.2.3.2 Scenario 2 58

4.2.3.3 Scenario 3 59

4.2.3.4 Scenario 4 61

4.2.3.5 Summary of the Third Experiment . . 62

4.2.4 Results of the Noise and Coupling Measurements . 64

4.2.4.1 Receiver Noise 64

4.2.4.2 Noise and Coupling in the Receiver for the Monostatic Case 65

4.2.4.3 Relation between SNR and Direction Finding Accuracy 66

5 CONCLUSION AND FUTURE STUDIES 67

REFERENCES 69

APPENDICES

A MATLAB CODE FOR THE DF ALGORITHM 73

LIST OF TABLES

TABLES

Table 4.1 Results of the DF Experiment for LFM Based FDA at the Center Frequency of 5.88 GHz, 25% Bandwidth 55

Table 4.2 Results of the Monostatic DF Experiment for LFM Based FDA for the Short Range at the Center Frequency of 5.88 GHz, 25% Bandwidth . . 63

Table 4.3 Results of the Monostatic DF Experiment for LFM Based FDA for the Long Range at the Center Frequency of 7.84 GHz, 15% Bandwidth . . 63

Table 4.4 Results of the DF Experiment for LFM Based FDA at the Center Frequency of 5.88 GHz, 25% Bandwidth with an extra attenuator in the receiver 66

LIST OF FIGURES

FIGURES

Figure 2.1 Illustration of the series fed aperture that is used for beam steering for frequency scanning radars 6

Figure 2.2 Schematic of an FDA 8

Figure 3.1 LFM frequency regime 14

Figure 3.2 LFM based FDA setup 15

Figure 3.3 Receiver FDA 17

Figure 3.4 Omnidirectional LFM transmitter 18

Figure 3.5 Sawtooth wave modulated signal 18

Figure 3.6 Transmitter structure for the method 1 19

Figure 3.7 Receiver structure for the method 1 20

Figure 3.8 Frequencies of the LO and the received pulse of the LFM based FDA 21

Figure 3.9 Transmitter structure for the method 2 24

Figure 3.10 Receiver structure for the method 2 25

Figure 3.11 Division patterns from boresight to $\theta = 45^o$ 27

Figure 3.12 Division patterns from boresight to $\theta = -45^o$ 28

Figure 4.1 Sketch of the setup in the first experiment 33

Figure 4.2 Sketch of the setup in the second experiment 34

Figure 4.3 Sketch of the setup in the third experiment 35

Figure 4.4 Photograph of the transmitter 36

Figure 4.5 Photograph of the receiver array 37

Figure 4.6 Photograph of the reflector 38

Figure 4.7 Photograph of the magic tee 40

Figure 4.8 Phase imbalance between the measurements of J1 to $\sum$ port and J2 to $\sum$ port 41

Figure 4.9 Phase deviation from 180^o between the measurements of J1 to Δ port and J2 to Δ port 41

Figure 4.10 Phase imbalance between the measurements of J1 to $\sum$ port and J2 to $\sum$ port after the compensation 42

Figure 4.11 Phase deviation from 180^o between the measurements of J1 to Δ port and J2 to Δ port after the compensation 42

Figure 4.12 Received signal for the center frequency of 5.88 GHz, 25% bandwidth and $\theta = 0^o$ for the first experiment 44

Figure 4.13 Received signal for the center frequency of 5.88 GHz, 25% bandwidth and $\theta = 30^o$ for the first experiment 45

Figure 4.14 Received signal for the center frequency of 7.84 GHz, 15% bandwidth and $\theta = 0^o$ for the first experiment 47

Figure 4.15 Received signal for the center frequency of 7.84 GHz, 15% bandwidth and $\theta = -15^o$ for the first experiment 48

Figure 4.16 Received signal from the sum channel for the center frequency of 5.88 GHz, 25% bandwidth and $\theta = 0^o$ for the second experiment 49

Figure 4.17 Received signal from the difference channel for the center frequency of 5.88 GHz, 25% bandwidth and $\theta = 0^o$ for the second experiment 49

Figure 4.18 Received signal from the sum channel for the center frequency of 5.88 GHz, 15% bandwidth and $\theta = -20^o$ for the second experiment 50

Figure 4.19 Received signal from the difference channel for the center frequency of 5.88 GHz, 15% bandwidth and $\theta = -20^o$ for the second experiment 51

Figure 4.20 Received signal from the sum channel for the center frequency of 7.84 GHz, 15% bandwidth and $\theta = 15^o$ for the second experiment 52

Figure 4.21 Received signal from the difference channel for the center frequency of 7.84 GHz, 15% bandwidth and $\theta = 15^o$ for the second experiment 52

Figure 4.22 Received signal from the sum channel for the center frequency of 5.88 GHz, 25% bandwidth and $\theta = 25^o$ for the second experiment 53

Figure 4.23 Received signal from the difference channel for the center frequency of 5.88 GHz, 25% bandwidth and $\theta = 25^o$ for the second experiment 54

Figure 4.24 Received signal for the short range measurement from the sum channel for the center frequency of 5.88 GHz, 25% bandwidth and $\theta = 20^o$ for the third experiment 57

Figure 4.25 Received signal for the short range measurement from the difference channel for the center frequency of 5.88 GHz, 25% bandwidth and $\theta = 20^o$ for the third experiment 57

Figure 4.26 Received signal for the short range measurement from the sum channel for the center frequency of 7.84 GHz, 15% bandwidth and $\theta = -20^o$ for the third experiment 58

Figure 4.27 Received signal for the short range measurement from the difference channel for the center frequency of 7.84 GHz, 15% bandwidth and $\theta = -20^o$ for the third experiment 59

Figure 4.28 Received signal for the long range measurement from the sum channel for the center frequency of 5.88 GHz, 25% bandwidth and $\theta = 20^o$ for the third experiment 60

Figure 4.29 Received signal for the long range measurement from the difference channel for the center frequency of 5.88 GHz, 25% bandwidth and $\theta = 20^o$ for the third experiment 60

Figure 4.30 Received signal for the short range measurement from the sum channel for the center frequency of 7.84 GHz, 15% bandwidth and $\theta = -20^o$ for the third experiment 61

Figure 4.31 Received signal for the short range measurement from the difference channel for the center frequency of 7.84 GHz, 15% bandwidth and $\theta = -20^o$ for the third experiment 62

Figure 4.32 Receiver noise 64

Figure 4.33 Signal in the receiver without a target 65

LIST OF ABBREVIATIONS

LFM	linear frequency modulation
FDA	frequency diverse array
DF	direction finding
CW	continous wave

CHAPTER 1

INTRODUCTION

FDA is a recent concept with various features that are distinct from the conventional arrays. It is a promising technology and it is getting its place in the new radar designs. Diversity brings extra information for the radars and it can be in the form of spatial, polarization, or frequency diversity [1]. Spatial and polarization diversities are difficult to implement for the practical systems where the polarization diversity mostly found its place only in the applications in the rain clutter [1]. However, frequency diversity is easy to implement because of the improvements in solid state RF sources. It was not straightforward to implement frequency hopping or scanning with the use of RF tube sources. Therefore, as the solid state RF technology develops, wideband phased array radar designs can be easily realized. Consequently, advantages of this type of arrays such as beam steering, controlling illumination of antenna aperture, and operating with multiple functions are taking the foreground.

FDA is a special type of phased array which takes attention with its dynamic properties. It differs from the frequency hopping and scanning techniques with the feature that all antenna elements have unique frequencies. Instantaneous bandwidth is distributed among the aperture which brings the waveform diversity. It is firstly introduced by [2].

LFM based FDA is a subset of FDA family. It was proposed by [3] for the practical issues. After that, it is studied by [4] which further reveals its advantages. LFM based FDA has the most of the advantages of FDA. Beside of these, it is possible to reach large instantaneous bandwidth with a single source. Therefore, it is easy to reach ultra-high range resolutions. Also, it allows to change modulation parameters which gives way to multiple radar operations. These advantages feature LFM based FDA as a future technology.

DF is one of the main operations for the most of the tracking radars. In order to take precaution for electronic countermeasures, it is very important to implement monopulse DF. Monopulse DF decreases the operation time which is important to take action within a few milliseconds. In addition, if the target is fast and maneuvering, it is almost impossible to detect its position with the methods other than monopulse DF.

There are lots of monopulse DF techniques for the pulse radars. Amplitude comparison and interferometry are the most popular and conventional techniques [5]. However, DF techniques for the CW radars are limited. In addition, range-angle coupling in FDA radars and dynamic properties of the operation make the monopulse DF techniques complicated for this type of radars. In this study, two monopulse DF methods for LFM based FDA are explored. Advantages and disadvantages of these methods are discussed. Experiments regarding one of the methods are presented with the results and relevant discussions.

In the second chapter of the thesis, literature is surveyed. The scanning radars are reviewed and DF methods for this type of radars are searched. After that, FDA radar is reviewed with the mathematical expressions. Recent studies on range-angle decoupling for FDA are given. Absence of a method for monopulse DF in FDA radars is stressed in this part.

In the third chapter, LFM based FDA concept is reviewed with the mathematical derivations. Differences between FDA and LFM based FDA concepts are given. Two DF methods are presented with the relevant discussions. Possible improvements are stated.

Experimental setup for the implementation of one of the given DF methods is introduced in the fourth chapter. Encountered difficulties in the implementation phase are stated with the approved solutions. Results of the experiments are presented. Comparisons with the expectations are made.

To conclude, reasons for this research are mentioned. Outcomes of the work are stressed. Future studies to improve this research are stated.

References are given after conclusion and future studies.

As the last part of the thesis in the appendix section, DF algorithm that is used in these experiments is given.

CHAPTER 2

FREQUENCY SCANNING RADAR AND FREQUENCY DIVERSE ARRAY IN LITERATURE AND MOTIVATION

2.1 Frequency Scanning Radar

2.1.1 Brief Review of Frequency Scanning Radar

Frequency scanning is one of the simple solutions to scan beam [6]. It was very frequent to use this method, especially in one angular coordinate [1]. Beam steering is simply done with the changing frequency. Consider a series fed aperture as in Figure 2.1.

The frequency of the excitation affects the phase difference between the consecutive antennas directly with the relation,

$$\phi = 2\pi f \ell / v \tag{2.1}$$

where f is the frequency of the excitation, ℓ is the length of the connection between consecutive antennas, and v is the velocity of propagation. If we assume that beam points to broadside at the excitation wavelength of λ_o, equation 2.2 gives the relation between the wavelength of the excitation, λ, and the beam direction θ_o [1].

$$sin\theta_o = \frac{\ell}{d}\left(1 - \frac{\lambda}{\lambda_o}\right) \tag{2.2}$$

There are some disadvantages of this method. It restricts the use of bandwidth for other purposes. Therefore, high range resolution cannot be obtained. In addition, radar can be exposed to electronic counter measures; because, bandwidth is narrow

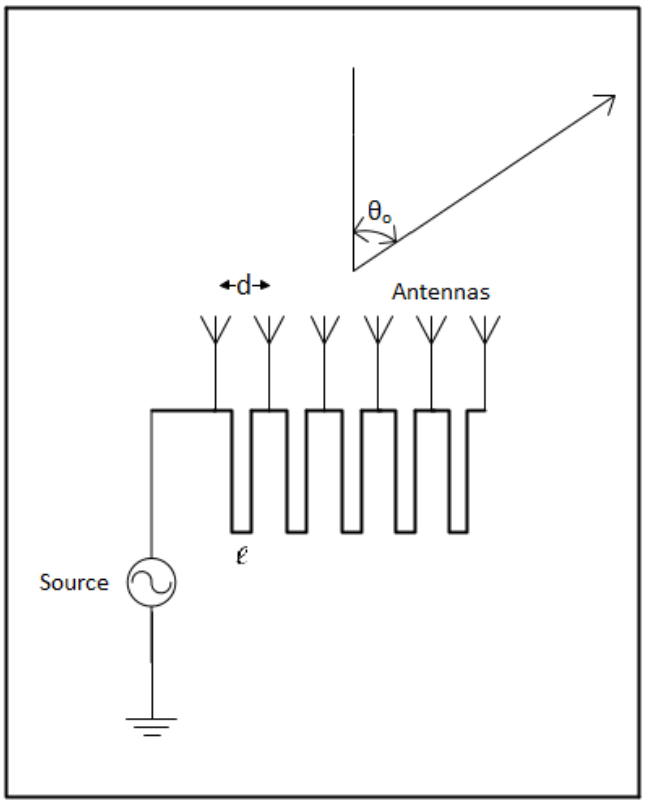

Figure 2.1: Illustration of the series fed aperture that is used for beam steering for frequency scanning radars

on each look-angle. Beside these, it is difficult to implement pulse-to-pulse frequency agility [1].

2.1.2 Monopulse Direction Finding for Frequency Scanning Radar

In general, sequential lobing is the common method for DF for the frequency scanning radars. It is easy to implement with two slightly distinct operation frequencies and it is enough for lots of applications [6]. There are some techniques that are used for monopulse DF for frequency scanning. Parallel-fed, tandem-fed monopulse arrays and dummy-snake monopulse technique are some of them [6]. In these techniques, appropriate sum and difference patterns are attempted to form. Inherently, asymmetries on the feed lines constitute problems. These asymmetries are necessary for the frequency scanning, but they may create amplitude imbalance which may deteriorate the shape of the patterns. This problem degrades DF performance of the

pulse radar. However, degradation in the performance of CW radars is not as much as pulse radars. Reason of this is that beam scans all points in angle in CW radars. The same situation is valid for the CW LFM based FDA radar and details of this discussion will be stated in the proceeding sections of the thesis. Therefore, some of the frequency scanning antennas stated in [6] can still be used for the CW radars as in this study. Dummy-snake frequency scanning monopulse antenna is used in this study for the experiments, since it allows using of magic tee.

There are also other types of frequency scanning monopulse antenna in literature. One of them is slotted-waveguide antenna which brings low loss for beam-forming networks. In [7], sum and difference patterns with low-sidelobes are obtained without additional loss. In [8], frequency-controlled scanning monopulse antenna is demonstrated and possible implementation scheme with waveguides is given. It allows the combination of dualplane frequency-sensitive scanning and dual plane monopulse DF.

2.2 Frequency Diverse Array

2.2.1 Brief Review of Frequency Diverse Array

FDA is a recent approach that is proposed by [2] to improve the time-modulated array designs. In order to reach ultra-low sidelobes, time-modulated arrays were suggested by [9]. In order to form desired antenna patters, on-off RF switches are used in a predetermined sequence. In FDA, there is progressive frequency shift between the consecutive radiators. It forms range-angle-time dependent beam [2].

Figure 2.2 demonstrates the basic structure of an FDA.

There are other types of implementation schemes for FDA [10, 11]. But Figure 2.2 is enough to understand the main idea.

For classical phased arrays, when progressive phase shift is applied between the consecutive antennas, beam can be tilted in accordance with this phase. In FDA, progressive frequency shift creates continuously increasing phase steps between the

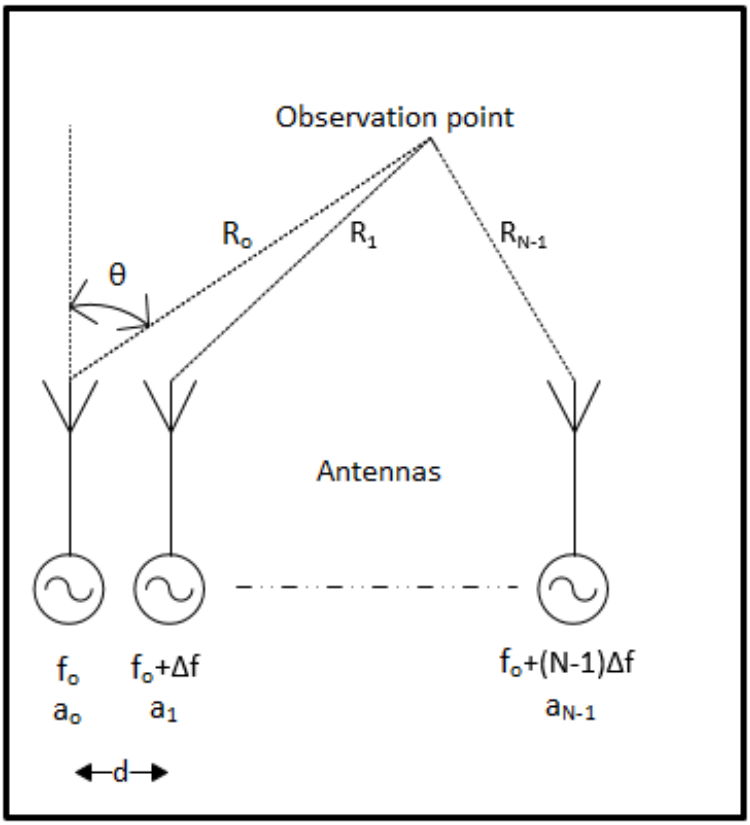

Figure 2.2: Schematic of an FDA

consecutive antennas which result in continuously scanning beam.

Consider an N-element uniform array with progressive frequency shift, Δf and inter-element distance of d as in Figure 2.2.

E-field of this type of array can be written as:

$$E = \sum_{n=0}^{N-1} \frac{a_n f_e(2\pi f_o + 2\pi n\Delta f)}{R_n} e^{j2\pi(f_o+n\Delta f)(t-\frac{R_n}{c})} \tag{2.3}$$

where a_n is the weighting for the nth element, f_o is the frequency of the leftmost element, f_e is the element factor, R_n is the range between the observation point and the nth element, t is the time and c is the velocity of light.

Some appropriate approximations will clarify the expressions. Note that approximations in phase term are made for time-independent residuals.

Let's assume uniform weightings for the elements, $a_n = 1$ and assume that element patterns are frequency independent, $f_e(2\pi f_o + 2\pi n\Delta f) \cong f_e(2\pi f_o)$. Note that, in order to decrease sidelobes, it is possible to weight antennas. In addition, if we make far field approximation for the range; in the phase term of the expression, we have $R_n \cong R_o - ndsin\theta$ and in the amplitude part of the expression, we have $R_n \cong R_o$. Then equation 2.3 can be written as

$$E = \frac{f_e(2\pi f_o)}{R_o} e^{j2\pi f_o(t-\frac{R_o}{c})} \sum_{n=0}^{N-1} e^{jn\phi} \tag{2.4a}$$

$$\phi = 2\pi\Delta f(t - \frac{R_o}{c}) + 2\pi(f_o + n\Delta f)\frac{dsin\theta}{c} \tag{2.4b}$$

If the instantaneous bandwidth of the array is much smaller than the smallest operation frequency of the array elements, $(N-1)\Delta f << f_o$, then ϕ in equation 2.4b can be rewritten as in equation 2.5.

$$\phi = 2\pi\Delta f(t - \frac{R_o}{c}) + \frac{2\pi f_o dsin\theta}{c} \tag{2.5}$$

Now we can extract the summation term of equation 2.4a, and rewrite the E-field as

$$E = \frac{f_e(2\pi f_o)}{R_o} e^{j2\pi f_o(t-\frac{R_o}{c})} e^{j\frac{N-1}{2}\phi} \frac{sin\frac{N\phi}{2}}{sin\frac{N}{2}} \tag{2.6}$$

In equation 2.6, $\frac{sin\frac{N\phi}{2}}{sin\frac{N}{2}}$ term creates amplitude modulation with respect to range, time and $sin\theta$. Relevant parameters of the modulation are extracted in [3].

There are lots of recently revealed advantages of FDA. It is resistant to multipath interferences [2]. It has various advantages for synthetic aperture radar imaging applications [12]. In addition, FDA is convenient for electronic counter-counter measures [13]. In order to use FDA as radar, [14] gives valuable information about the limits for estimating direction, range and velocity.

2.2.2 Range-angle Coupling of Frequency Diverse Array

In order to measure the angle accurately, range-angle coupling should be solved in FDA radars. Therefore, current researches focus on this problem and various researchers propose different solutions for this. In [10], using two different frequency increments is proposed. [15] uses double pulse. Angular position of the target is found by the conventional phased array approach. Then, frequency increments between the consecutive antennas are arranged accordingly to find the range of the target. It is proved that this method increases the direction accuracy with respect to conventional phased array approach. In [16], two subarrays with different frequency increments are used to solve the range-angle coupling. In [17], transmit subaperturing is used with the convex optimization which both solve the range-angle coupling and focus the transmit beam. In [18], two solutions are summarized. First one is to use constant frequency increments on nonuniform linear array; other one is to use irregular frequency increments on uniform linear array. In [19], second solution is implemented. Costas-sequence modulated frequency distribution is proposed on the same article. In [20], novel antenna array, random FDA, is introduced to solve this problem. And finally in [21], novel method to solve this problem is proposed. Two transmitting pulses with Δf and $-\Delta f$ frequency increments are used. Time difference between the received pulses is shown to be proportional with $sin\theta$ where θ is the angle of the target.

Proposed methods give the solution for the range-angle coupling of FDA. Advantage of using LFM based FDA is to have a synchronous signal for each FM period. Therefore, using this signal, one can easily decouple range and angle in monopulse. For this reason, monopulse DF using LFM based FDA radar can be implemented without abandon the advantages of frequency diversity. In this thesis, two DF methods are presented with the experimental results.

2.3 Summary of the Study

Firstly, FDA concept was reviewed and necessary mathematical formulations were re-examined as in this chapter. After the initial derivations of FDA, focus was on

the LFM based FDA which is proved in [3] as a practical system to realize FDA. Mathematical derivations regarding the LFM based FDA were done. After that, two DF methods were constructed. Their advantages and disadvantages were discussed with respect to conventional DF methods. The purpose of this study is to verify the assumptions with experiments. Therefore, three experiments were performed in the anechoic chamber. DF algorithm was developed in MATLAB. Most of the work was gathered together in [22]. Finally, improvements for these methods were discussed.

2.4 Organization of the Thesis

In chapter 3, mathematical derivations of LFM based FDA are done. Two DF methods for LFM based FDA radars are presented. Possible improvements are discussed.

In chapter 4, experiments regarding one of the DF methods are presented with the results.

Finally in chapter 5, conclusion is given with the possible future studies.

CHAPTER 3

LINEAR FREQUENCY MODULATION BASED FREQUENCY DIVERSE ARRAY ANALYSIS AND DIRECTION FINDING METHODS

3.1 Linear Frequency Modulation based Frequency Diverse Array Analysis

In this section, in order to form a basis for DF methods, mathematical expressions of LFM based FDA are derived. Firstly, setup is introduced. After that, derivations are given.

3.1.1 Setup of the Array

In order to implement FDA practically, LFM based FDA setup is proposed by [3]. In this novel method, array is fed by a single LFM source which has a frequency regime as in Figure 3.1

This behavior can be modeled as in equation 3.1.

$$\omega_s = \omega_o + mt \tag{3.1}$$

where ω_s is the angular frequency of the source, ω_o is the initial angular frequency, m is the slope of the angular frequency regime and t is the time. In the proposed method, this source excites the aperture where progressive delay is introduced between the antenna elements. Array setup is given in Figure 3.2.

As it is inferred from Figure 3.2, frequencies of antennas are changing and the center frequency of the aperture is increasing as time advances. This is the substantial

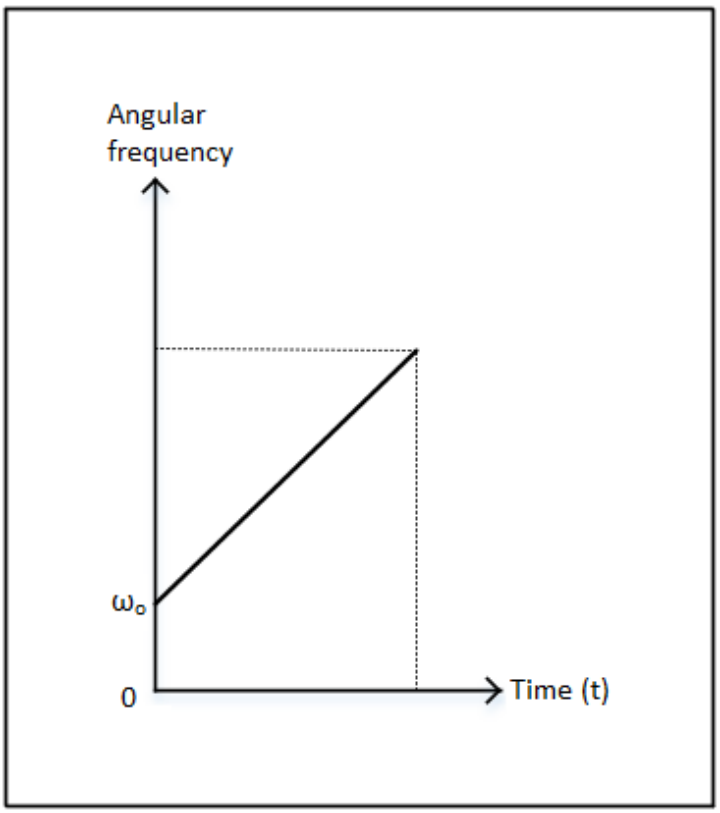

Figure 3.1: LFM frequency regime

originality of LFM based FDA.

3.1.2 Mathematical Derivations

E-field of an N-element LFM based FDA can be written as in equation 3.2.

$$E = \sum_{n=0}^{N-1} \frac{a_n f_e(\omega_o + m(t - nt_d))}{R_n} e^{-j(\omega_o + m(t-nt_d))\frac{R_n}{c}} e^{j(\omega_o(t-nt_d)+\frac{m}{2}(t-nt_d)^2)} \tag{3.2}$$

where a_n is the weighting for nth element, f_e is the element pattern, R_n is the range between the observation point and nth antenna, t_d is the delay between the consecutive antenna elements, c is the velocity of light.

In order to simplify the equations, uniform fed aperture is assumed, $a_n = 1$. Note that, in order to decrease sidelobes, it is possible to weight antennas. And element

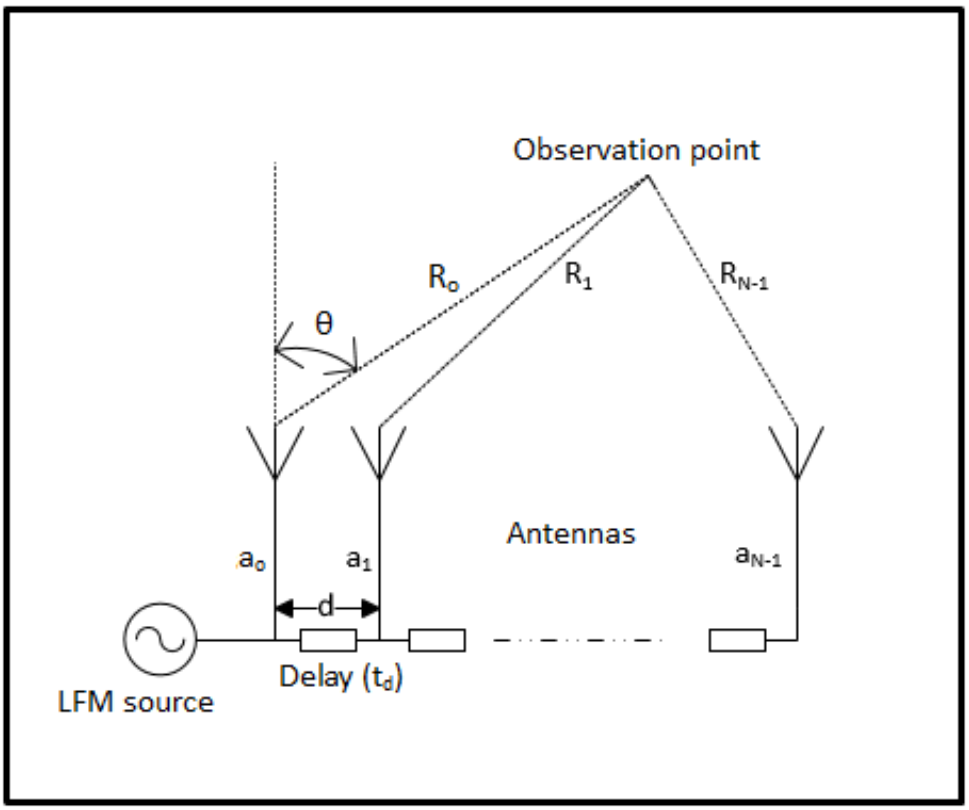

Figure 3.2: LFM based FDA setup

patterns are ignored for further simplification, $f_e = 1$. In addition R_n is taken as R_o in the denominator and as $R_o - ndsin\theta$ on the phase term where d is the distance between the elements. After these simplifications E-field can be written as in equation 3.3.

$$E = \sum_{n=0}^{N-1} \frac{e^{-j\frac{1}{c}(\omega_o + mt - mnt_d)(R_o - ndsin\theta)}}{R_o} e^{j(\omega_o t - \omega_o nt_d + \frac{m}{2}t^2 - mtnt_d + \frac{n^2 t_d^2 m}{2})} \tag{3.3}$$

In the exponential terms, it is possible to ignore some time independent small terms. Sum of the phase terms of the exponentials can be expanded as:

$$\begin{aligned} \phi = \frac{\omega_o R_o}{c} + \frac{\omega_o ndsin\theta}{c} - \frac{mtR_o}{c} + \frac{mtndsin\theta}{c} + \frac{mnt_d R_o}{c} - \frac{mn^2 t_d dsin\theta}{c} \\ +\omega_o t - \omega_o nt_d + \frac{mt^2}{2} - mtnt_d + \frac{n^2 t_d^2 mc}{2} \end{aligned} \tag{3.4}$$

If we assume that range is larger than the aperture, $R_o >> \frac{nct_d}{2}$, last term in equation

3.4 can be ignored. And it is possible to ignore $\frac{mn^2 t_d dsin\theta}{c}$ where it is time independent and small term. It is proved in [3] that these terms don't alter the beamshape seriously. Finally ϕ can be written as in equation 3.5.

$$\phi = \frac{\omega_o R_o - mtR_o + \omega_o tc + \frac{mt^2 c}{2}}{c} + n(\frac{\omega_o dsin\theta + mtdsin\theta + mt_d R_o - \omega_o t_d c - mtt_d c}{c}) \tag{3.5}$$

Using equation 3.5, E-field can be written as in equation 3.6.

$$E \cong \frac{1}{R_o} e^{j(\omega_o(t-\frac{R_o}{c})+\frac{mt^2}{2}-\frac{mR_o t}{c})} \sum_{n=0}^{N-1} e^{jn((\frac{\omega_o+mt}{c})(dsin\theta-ct_d)+\frac{mt_d R_o}{c})} \tag{3.6}$$

when the phase of the sum term is proportional with n, it is possible to write it as in equations 3.7a and 3.7b.

$$E \cong \frac{1}{R_o} e^{j(\omega_o(t-\frac{R_o}{c})+\frac{mt^2}{2}-\frac{mR_o t}{c})} \frac{sin(\frac{N\varphi}{2})}{sin(\frac{\varphi}{2})} e^{j\frac{N-1}{2}\varphi} \tag{3.7a}$$

$$\varphi = (\frac{\omega_o + mt}{c})(dsin\theta - ct_d) + \frac{mt_d R_o}{c} \tag{3.7b}$$

Note that, equation 2.6 and equation 3.7a are very similar. Modulation term in equation 3.7a, $\frac{sin(\frac{N\varphi}{2})}{sin(\frac{\varphi}{2})}$, brings the same FDA characteristics in LFM based FDA. When either R_o, $sin\theta$, or t is variable and the remaining two of them are fixed, amplitude modulation can be observed with respect to the variable one.

3.2 Monopulse Direction Finding Methods for Linear Frequency Modulation based Frequency Diverse Array and Possible Improvements

LFM based FDA is CW array with dynamic scanning properties. Therefore, when it operates as radar, DF methods for this type of CW radar are different than the conventional methods.

Monopulse DF for LFM based FDA can be implemented with a receiver FDA and an omnidirectional LFM transmitter. Receiver FDA is a series fed aperture where the

beam-former is combined to a receiver as it is shown in Figure 3.3. In order to form sum and difference patterns in the receiver, antenna weightings should be arranged accordingly. In Figure 3.3, a generic receiver is demonstrated with the antenna weightings and N receiver channel. In the following sections, in order to implicate the sum and difference channels, the receiver part will be simply demonstrated with a magic tee. In this thesis, monostatic radar is concerned. It is assumed that the transmitter and receiver antennas are at the same point. All derivations are done with this assumption.

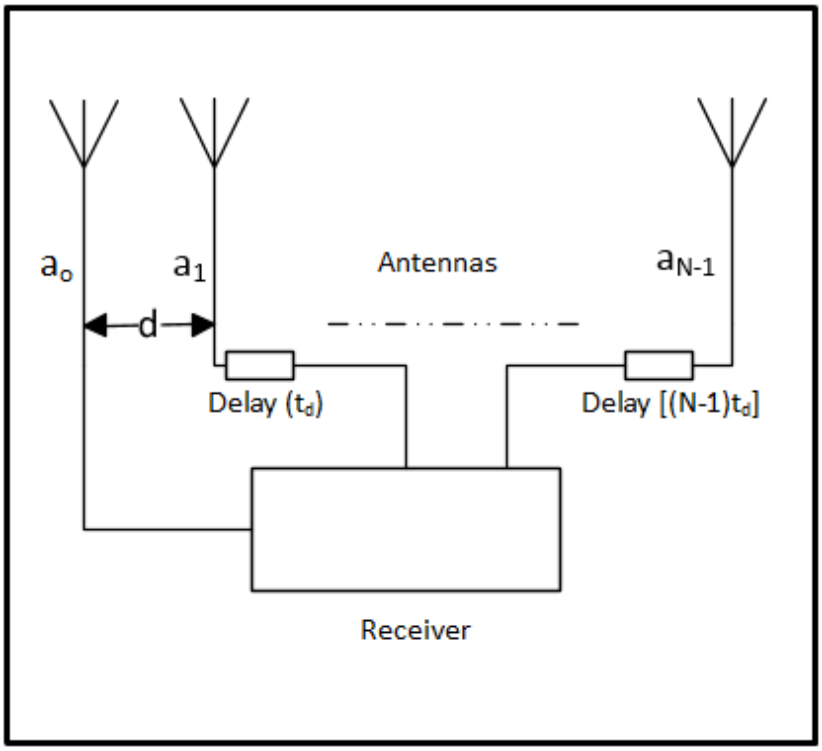

Figure 3.3: Receiver FDA

Omnidirectional LFM transmitter is simply an LFM source with an omnidirectional transmitter antenna as it is shown in Figure 3.4. In order to realize the LFM frequency regime, transmitted signal can be frequency modulated by a sawtooth wave for a practical system as it is shown in Figure 3.5.

There are two proposed methods to implement monopulse DF for LFM based FDA in this thesis. Their structures basically include the aforementioned transmitter and receiver structures, but receiver structures of these methods are different from each

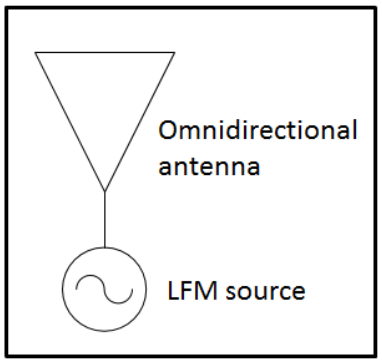

Figure 3.4: Omnidirectional LFM transmitter

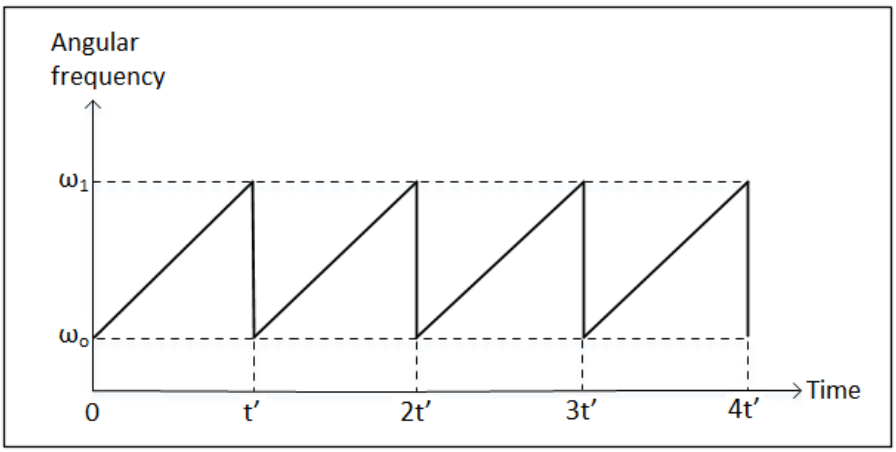

Figure 3.5: Sawtooth wave modulated signal

other in detail. Particular RF front-ends are also given in the proceeded sections.

3.2.1 Method 1: Using Time Data

In order to explain the method clearly, transmitter and receiver structures are given in Figure 3.6 and 3.7 respectively.

Received signals are the peaks of the E-field in equation 3.7a. Peaks of the E-field are formed when equation 3.7b satisfies the relation in equation 3.8,

$$(\frac{\omega_o + mt}{c})(dsin\theta - ct_d) + \frac{mt_d R_o}{c} = 2\pi\ell \tag{3.8}$$

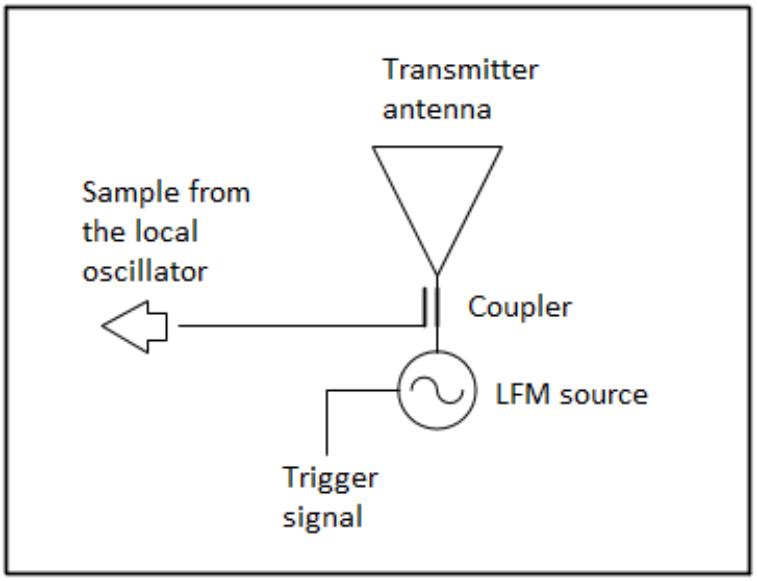

Figure 3.6: Transmitter structure for the method 1

where $\ell = 0, \mp 1, \mp 2...$ In this equation, time of arrival, t, angle of arrival, θ, and range, R_o are the unknowns. In order to find one of them, the remaining two should be found. Therefore, accuracies of these unknowns are related to each other. Consequently, if range or time of arrival will be found with the improved accuracy, angle of arrival can be found with the accuracy of fraction of beamwidth.

In subsection 3.1.2, amplitude modulation on the received signal was derived. As it is understood from the expressions, although the operation was CW, received signal was pulsed. Range and time of arrival will be fetched with the help of the parameters of this received pulse.

In order to find the range, received pulse can be mixed with the LO signal. Frequency difference between the received pulse and the LO signal is proportional with the range and doppler [3, 23–26]. The operation is similar with that is used for conventional LFMCW radar. Only difference between the operations is that received signal in conventional LFMCW radar is CW where the received signal in LFM based FDA is pulsed. In order to express the idea behind the method to find range, instantaneous frequencies of the received pulse signal and LO signal are given in Figure 3.8. Notice that the parameters of the modulation on the transmitted signal have the same convention with Figure 3.5.

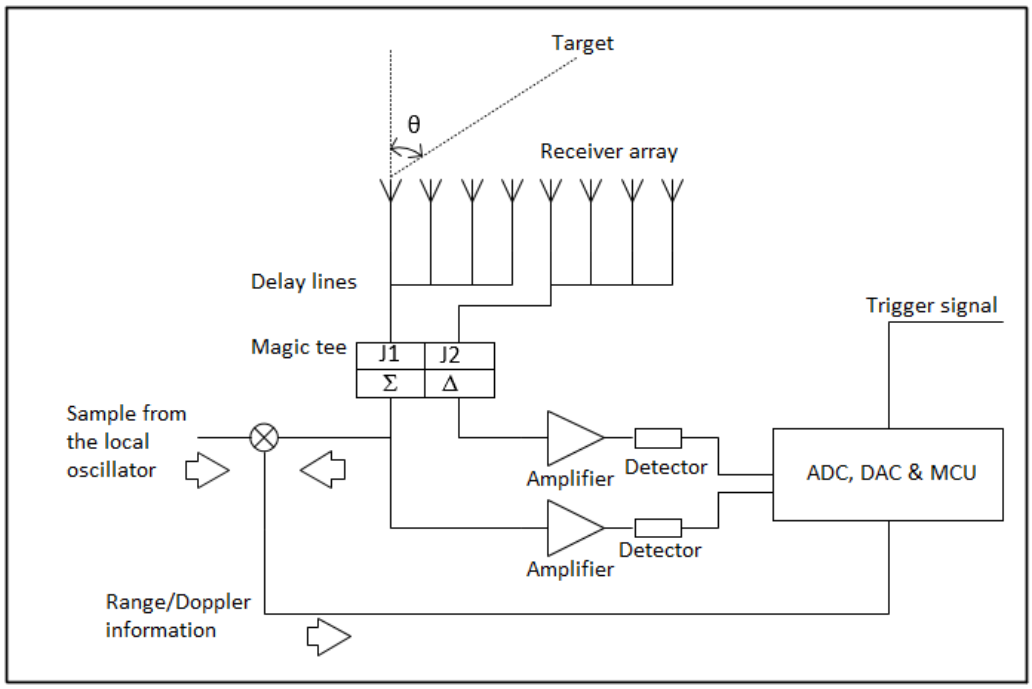

Figure 3.7: Receiver structure for the method 1

As it is inferred from Figure 3.8, delay (range) contributes to frequency difference (IF) between the LO and received pulse as it shifts the received pulse on the time axis. At the same time, doppler also creates frequency difference as it shifts the received pulse on the frequency axis. Notice that, frequency difference is not affected by the angle of arrival. As it is explained in the preceded sections, beam is scanning as the frequency advances in LFM based FDA. Since our reference is LO, frequency difference is only affected by delay or doppler.

Contribution of the doppler to the IF signal is much smaller than that of the range. Therefore, one can ignore the doppler and find the range with one sweep. It is important to obtain range in one sweep since it corresponds to monopulse operation. If it is desired to find the radial velocity of the target, [3] gives valuable information. It is said that the doppler can be found from the slow time data as in the case of conventional radar. If one can take fourier transform of the consecutive pulses that corresponds to same range cell, it gives the doppler information.

After R_o is found, time of arrival remains to be fetched. Zero-point reference for the time of arrival is the starting point of the frequency modulation. In Figure 3.8, it

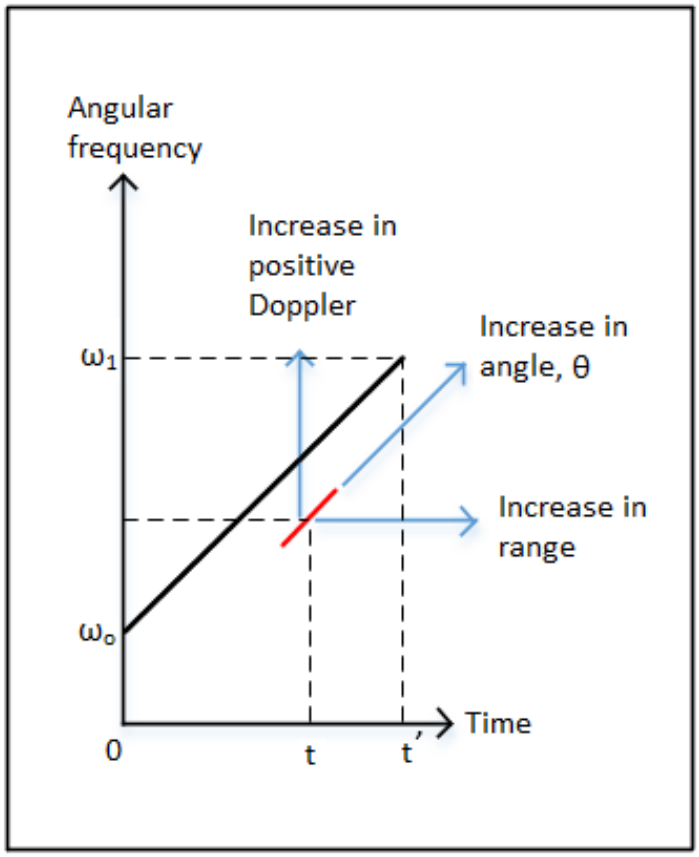

Figure 3.8: Frequencies of the LO and the received pulse of the LFM based FDA

is stated as $t = 0$. For the consecutive scans, time references are shown in Figure 3.5 as $t = 0, t', 2t' ...$ These instances are related to modulation parameters which are controllable and they can be used as trigger data to find the time of arrival. Note that the trigger signal in Figure 3.6 and 3.7 corresponds to this data.

Note that, in Figure 3.8, t corresponds to somewhere in the pulse. Remember that if the angle of arrival would be found with high accuracy, at least one of the other unknowns (R_o or t) should also be found with high accuracy. Therefore, in order to obtain accuracy of fraction of beamwidth for the angle of arrival, t should be found with the accuracy of fraction of pulse-width.

In order to find t accurately, instant of the peak of the received pulse should be found. Note that, noise disturbs the position of the peak. Therefore, errors mostly come from the noise. In addition, peak may not correspond to middle of the pulse. There are some factors that disturb the shape of the received pulse. Beamwidth is related to the

electrical size of the antenna aperture that is seen on the beam direction. Therefore, look-angle and the frequency content of the received pulse affect the beamwidth. Remember that for LFM based FDA, beam scanning is done with the changing frequency. Therefore, as the beam scans, beamwidth changes which also disturbs the received pulse. Nevertheless, there is no harm to use the peak of this asymmetrical received pulse as a reference, since it corresponds to the true position of the target.

For a noisy system, true position of the peak may not be found with the accuracy of fraction of pulse-width. This is the same situation with the conventional radar. Therefore, one should use specific beam-formers to overcome this situation.

One solution is to use sum and difference beam patterns as it is demonstrated in Figure 3.7 with a magic tee. It is always possible to use N channel receiver as it was demonstrated in Figure 3.3. In addition, one can use digital beam forming and can obtain various antenna patterns according to radar operation. Advantages of this will be explained in subsection 3.2.4. Here, in order to express the ideas behind the method, radar is demonstrated with its simple form.

When sum and difference patterns are used, one can obtain error signal with a simple division operation, as in the case of conventional radar. When difference pattern is divided by sum pattern, a deep sharp null is obtained. This null corresponds to exact location of the target. In pulse radar operation, since the beam doesn't scan all angles as in the CW radar, error signal corresponds to deviation from the null. However, since the operation is CW in LFM based FDA radar, error signal is obtained with its full span. Therefore, null is absolutely obtained. And null detection algorithm may be running in the signal processing algorithm.

Note that, it was explained that the beamshape of LFM based FDA may be disturbed because of some reasons. These distortions affect the sum and difference patterns together. However, peak of the sum pattern is formed at the same point with the null of the difference pattern. Therefore, distortions would not worsen the performance of the radar if noise-free system was concerned. However, in a noisy system, perfect null can not be obtained. And depending on null detection algorithm, distortions on the beamshape may mislead the algorithm and error on the null position may occur. Also in extreme scan angles (when the beam direction is close to $\theta = \mp 90^o$), where

the distortions on the beamshapes are dominant, target detection performance of the radar may also be affected by these heavily distorted beamshapes depending on the target detection algorithm. Therefore, target detection and null detection algorithms can be enhanced by some improvements. These improvements will be explained in subsection 3.2.4.

Null of the error signal gives the true location of the target. In Figure 3.8, t corresponds to instant of the null in the error signal. With the help of this information, t can be found with high accuracy. Consequently, angle of arrival can be found with the accuracy of fraction of beamwidth since they depend on each other with the relation 3.8.

3.2.2 Method 2: Using Frequency Content of the Received Signal

It was explained that the beam scans with changing frequency in LFM based FDA. And since the beam direction is directly related with the instantaneous center frequency of the antenna aperture, direction of the target can be directly found from this frequency. In LFM based FDA, for a one complete scan, all angles are scanned with an individual frequency component of the frequency band. If adequate band is used, it is possible to scan the same points in space with different frequencies in subsequent scans. This strengthens the radar against electronic counter measures. Also it is possible to decorrelate Rayleigh type clutters. Nevertheless, for a one scan, angle-frequency pairs are unique.

Note that, frequency steps between the consecutive antennas also affect the direction of the beam. This effect can also be taken into account since it is known parameter. However, it is also possible to ignore this effect as long as these increments are small with respect to the center frequency. Beam direction is determined by the instantaneous phase differences between the antennas. And center frequency is the main factor that creates these phase differences as the progressive delay lines are used. In this thesis, since the frequency increments between the antennas are small as in the practical systems, their effect on the direction of the beam is ignored in the proceeded deductions.

In order to clarify the method, transmitter and receiver structures are given in Figure 3.9 and 3.10 respectively. Method 1 and 2 have the same transmitter structure. It is given once again here for convenience.

Operation of the LFM based FDA is CW. Therefore, peak of the beam can not fail to illuminate the target. In the receiver, as the beam crosses over the target, pulse that is correlated with the beamshape appears in the sum channel. Since the beam scans as the center frequency shifts, this pulse has a frequency spectrum. Peak of this pulse corresponds to the peak of the beam. The frequency component at the peak of the pulse gives the true position of the target.

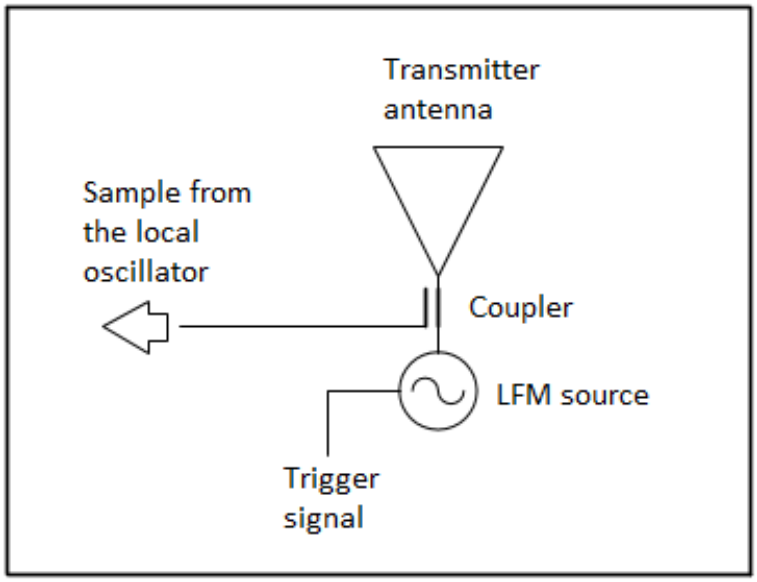

Figure 3.9: Transmitter structure for the method 2

In order to find the frequency component at the peak of the received pulse accurately, multiple channels or special beam formers should be used. Otherwise, it is not possible to detect the peak of the sum pattern in noisy environment. Therefore, magic tee is introduced as a simple beam-former in the receiver structure, Figure 3.10. One method to detect beam direction is to divide frequency transform of the difference pattern to frequency transform of the sum pattern. In the division spectrum, a frequency component that has minimum amplitude (ideally zero amplitude for a noiseless system) is directly related to the angle of arrival.

Range/doppler coupling creates errors on the measurements. However, as it is

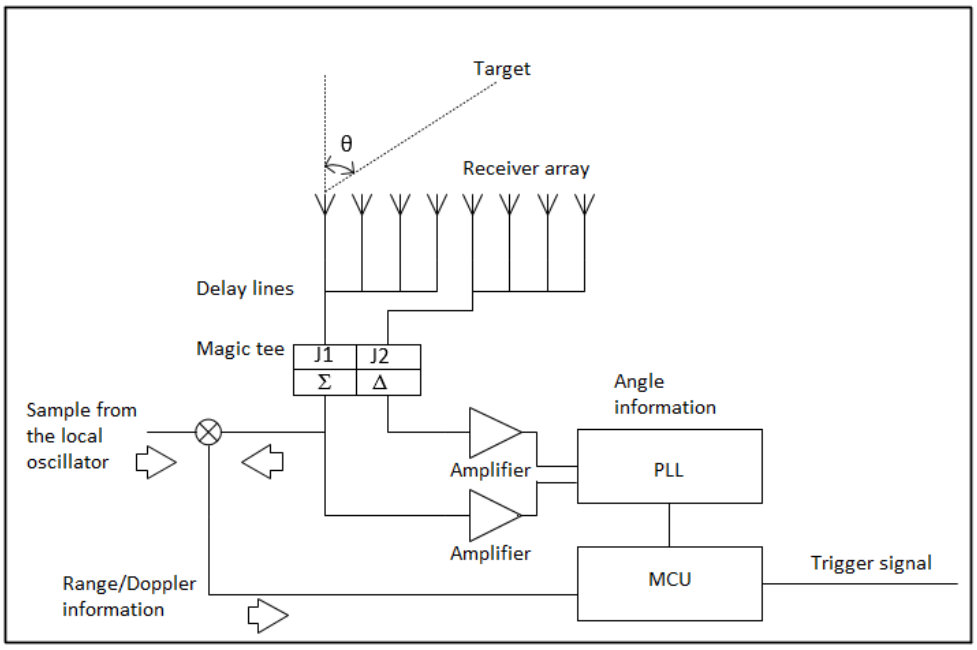

Figure 3.10: Receiver structure for the method 2

explained in the method 1, effect of the doppler is small compared to range in practical systems. Therefore, it is possible to ignore doppler.

3.2.3 Comparison of the Methods

The method 1 and 2 do not suggest independent solutions. In method 1, the solution of equation 3.8 was found. The unknowns of that equation were the time of arrival, t, angle of arrival, θ, and range, R_o. When R_o is found, trip time of the pulse can be revealed. After that, one can subtract the trip time from the time of arrival (starting instant of the FM is the reference point) so that instant of the formation of the pulse on the transmitting antenna can be found. Since the parameters of the frequency modulation are known, this instant associated with a frequency component on the frequency regime of the source. Time of arrival, t and range, R_o create sole solution for the angle in equation 3.8 and since they also create sole solution for the transmitted frequency, transmitted frequency can be directly associated with the angle of arrival.

Accuracies of the method 1 and 2 are the same since in both methods; main aim is to find the null of the difference pattern accurately. And since the beam-formers of both

of the methods are the same, magic tee, it is not expected to have different accuracy. In both methods, accuracy of fraction of a beamwidth is obtained with monopulse operation.

When method 1 and 2 are compared regarding to their implementability, it can be said that the frequency extraction for the method 2 is difficult to implement with respect to extraction of the time and range information for the method 1. Implementation of a PLL is not an easy task and method 1 may be preferred because of this reason. Note that the mixer in Figure 3.10 provides range and doppler information to the radar which are not required to find the angle of arrival with the method 2. However, for almost all radars, finding range and doppler is crucial. Therefore, one should still use mixer for the method 2.

3.2.4 Possible Improvements

The following improvements are given for monopulse DF for LFM based FDA. They can be implemented for both of the methods. They are generally used for conventional pulse radars. However, they are also compatible with LFM based FDA radar.

3.2.4.1 Pattern Recognition

It was mentioned in the method 1 that when the beam direction is close to $\theta = \mp 90^o$, detection performance of the radar may be severely degraded in noisy environment. Reason of that is to have asymmetrical beamshapes on the extreme angles. If the signal processing algorithm expects a symmetrical pulse shape, it may assume a null close to the center of the pulse in the difference channel. Therefore, null of the difference pattern may be estimated in an incorrect instance in noisy environment. Even the sum pulse may be missed if the algorithm searches for a symmetrical pulse in the noise. Target can be missed for this reason.

When the division pattern (difference pattern divided by the sum pattern) is concerned, asymmetries on the beamshapes also affect the division ratios. Division patterns from boresight to $\theta = 45^o$ are given in Figure 3.11. It is seen on the figure

that the angle between the wings of the division pattern is increasing as the beam strays from the boresight. The reason is that the antenna gain is decreasing on these angles. In addition, the wing away from the boresight is diverging faster than the other wing. This is due to have different frequency components in each scan angle. This dynamically affects the beam in the scanning. Similar results are obtained for the division patterns from boresight to $\theta = -45^o$ as it can be shown in Figure 3.12. Here, the divergence between the wings is more than the previous case, since the frequency is also decreasing as the beam scans through $\theta = -45^o$ which also contributes the decrease in the gain.

From Figure 3.11, it is calculated that for a target at $\theta = 25^o$, same levels of the error signal can be found on the look-angles of $\theta = 35^o$ and $\theta = 15.9^o$. Their difference from the deviation from the target angle is 0.9^o. If one calculates the beamwidth on those angles, it is found that there is approximately 1.65^o difference on those angles. Therefore, approximately $1.65^o/2 = 0.825^o$ deviation is expected between the same levels of the wings of the error signal which is close to the calculated value.

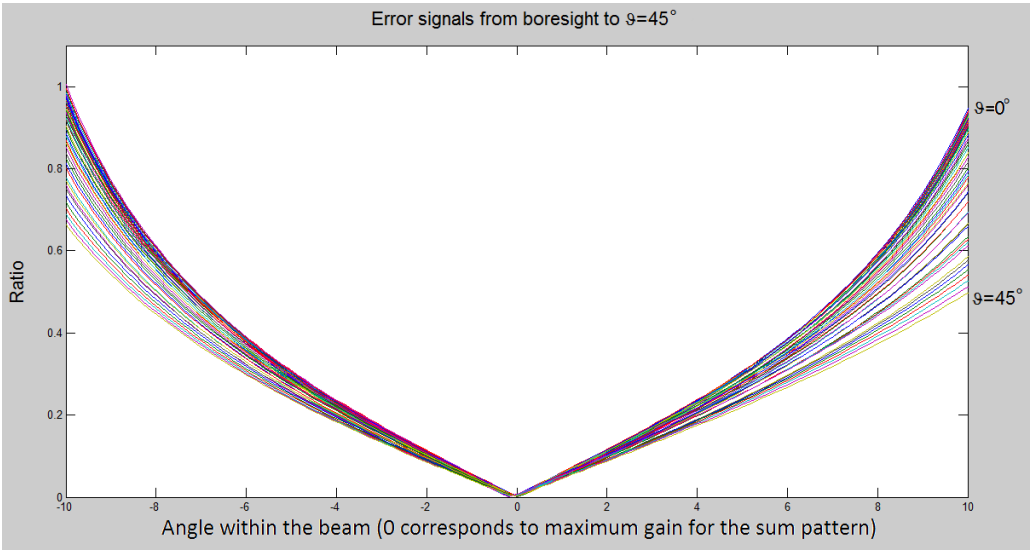

Figure 3.11: Division patterns from boresight to $\theta = 45^o$

Note that asymmetries on the beamshapes affect both sum and difference channels. Since sum and difference patterns differs only on the beam-forming network, null of the difference pattern forms at the same time with the peak of the sum pattern. Therefore, there would be no error on the angle of arrival as long as the null of the

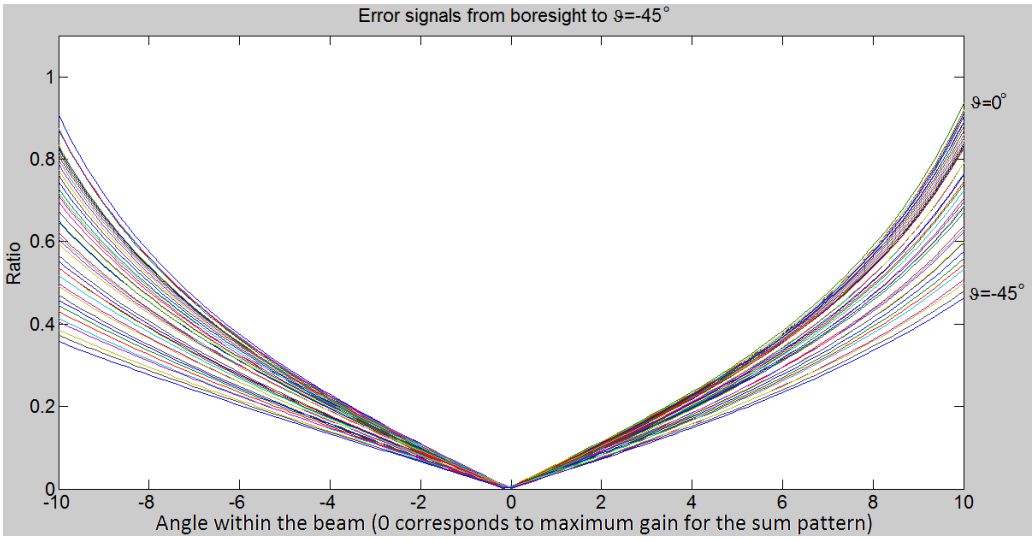

Figure 3.12: Division patterns from boresight to $\theta = -45^o$

division pattern (difference pattern divided by the sum pattern) is found on the exact instant.

In order to improve the detection performance of the radar, it is possible to use pattern recognition algorithms in the signal processing. Since the parameters of the frequency modulation and the characteristics of the array are known, sum and difference beamshapes can be calculated for any look-angles. And a look-up table for all scan angles can be embedded in the algorithm. Another solution is to measure the far field patterns of the array. Then, a look-up table can be filled with the measurements.

This improvement would enhance both the target detection performance and the null detection performance of the radar.

3.2.4.2 Using Low Sidelobe Antenna Pattern

There are different kinds of aperture illumination to obtain low sidelobe in the sum pattern. Taylor is one of them and it is implementable type of the Dolph-Chebyshev illumination. In the DF methods described in this thesis, there is only one receiver. However, in order to obtain optimum antenna patterns in the sum and different

channels, antenna weightings should be different. Generally, Bayliss illumination is used for the difference pattern. Therefore, it is possible to use two receivers with the different antenna weightings for the sum and difference patterns. One should be careful for the amplitude and phase imbalances in the two receiver chains.

The more general solution for the beam-shaping problems is digital beam forming which is also presented here.

3.2.4.3 Digital Beam Forming

Digital beam forming is a method to form multiple beams in the receiver. As in the conventional radars, digital beam forming in LFM based FDA brings lots of advantages. The main advantage of this method is to get rid of the beam-forming losses. When magic tee is used, power is split and it brings 3 dB loss to radar. However in digital beam forming, it is possible to have multiple simultaneous beams without degradation in SNR [1]. Analog beam formers also suffer from the losses that come from the weightings in low sidelobe antennas. However, digital beam formers are free from such losses.

There are numerous advantages of digital beam forming for LFM based FDA other than compensating losses [1]. These are briefly listed here:

- Errors in the weighting of the receiver array can be corrected by the digital beam forming, by use of a known scatterer.
- It allows to obtain low antenna sidelobes and compensate mutual coupling effects.
- It is possible to utilize adaptive nulling in order to protect radar from counter measures.
- Arrays are robust against the antenna element failures. However, when the low antenna sidelobe is concerned, failures of the array elements can seriously degrade the performance. By utilizing digital beam forming, compensation on the array pattern can be done.

- Flexible data rates enhance the performance of the radar for specific scenarios.
- It allows to utilize simultaneous multiple function.
- Improved noncooperative target recognition is possible.

3.2.4.4 Focusing on a Specific Angular Sector

It is said in the previous sections that scanning is done with the changing frequency for LFM based FDA. And frequency modulation of the LFM transmitter is controllable. Therefore, when radar operates in the surveillance mode and finds a target, it can start to sweep the specific region of its frequency band and in this way, it is possible to focus on a specific angular sector. Thus, radar can focus on a target and operate in tracking mode.

Transition between the operating modes brings extra flexibility to LFM based FDA radar and it doesn't require additional hardware.

CHAPTER 4

DIRECTION FINDING EXPERIMENTS FOR LINEAR FREQUENCY MODULATION BASED FREQUENCY DIVERSE ARRAY

In order to verify the theory behind the DF methods, an experimental setup was prepared. Three experiments were performed with this setup. Basic features of the LFM based FDA were observed and the theory behind the method 1 was proved with these experiments.

First experiment was performed to validate the setup and verify the basic characteristics of the LFM based FDA. In this experiment, there was no special beam former. A diode detector was used to observe pulse shapes and timings in various angle of arrivals.

In the second experiment, an experimental setup that is similar to the one in method 1 was constructed in the anechoic chamber as a one-way link. In order to process sum and difference channels, a signal processing algorithm was prepared which is also demonstrated in the appendix. It was shown in this experiment that $\mp 2^o$ direction accuracy for 15^o beamwidth can be obtained for 70^o azimuthal angular coverage in the anechoic chamber.

In the third experiment, monostatic LFM based FDA radar is tested with a 100 x 100 cm reflector. This experiment was performed for two different ranges. Signal processing algorithm was the same with the one that is used in the second experiment. DF is demonstrated successfully for both ranges within 70^o azimuthal angular coverage in the anechoic chamber.

Range was not found in these experiments. However, it was taken into account with poor accuracy in the calculations.

4.1 Experimental Setup

Sketches of the experimental setups for the first, second and the third experiment are given in Figure 4.1, Figure 4.2 and Figure 4.3 respectively. The structures were similar to those of method 1 and method 2. Transmitter structure was an LFM source with a horn antenna for the first and the second experiment. Photograph of the transmitter horn is shown in Figure 4.4. For the third experiment, a vivaldi antenna was used as a transmitter antenna. Receiver structure was an FDA with progressive delay lines (t_d = 0.51 ns) between the array elements for all experiments. It consists of 10 vivaldi antennas where the outer two of them were fill-antennas. These were used since the input impedances of the outer antennas are different in arrays. Distance between the antenna elements were d = 0.025 m. Photograph of the receiver array is shown in Figure 4.5. Range between the transmitter and the receiver was approximately 5 m for the first and the second experiment. Range between the reflector and radar was 3 m for the first trial of the third experiment and it was repeated for 5 m after the successful demonstration. Photograph of the reflector is shown in Figure 4.6.

Since the purposes of the experiments were different, there was a small distinction between the receiver chains. In the receiver chain of the first experiment, there was a single channel. In the second and the third experiment, magic tee was used and the measurements on the sum and difference channels were taken consecutively. Remaining elements of the chains were the same for all of the experiments. Low noise amplifier (LNA) was used as the first element. It prevents SNR from the further degradations in the proceeded stages. An equalizer was used after the LNA to compensate the frequency response of the system. After the equalizer, a power amplifier with 32.5 dB gain was used. Mixer was not used in these experiments. In order to convert the received RF signals to readable signals, a peak detector was used. Two channel oscilloscope was used where one of the channels displayed the received signal while the other was monitoring the trigger signal. Rising edges of the trigger signal correspond to starting instants of the frequency modulation while the falling edges correspond to the center frequency. A computer was used as a final element of the chains to store the data on the oscilloscope screen.

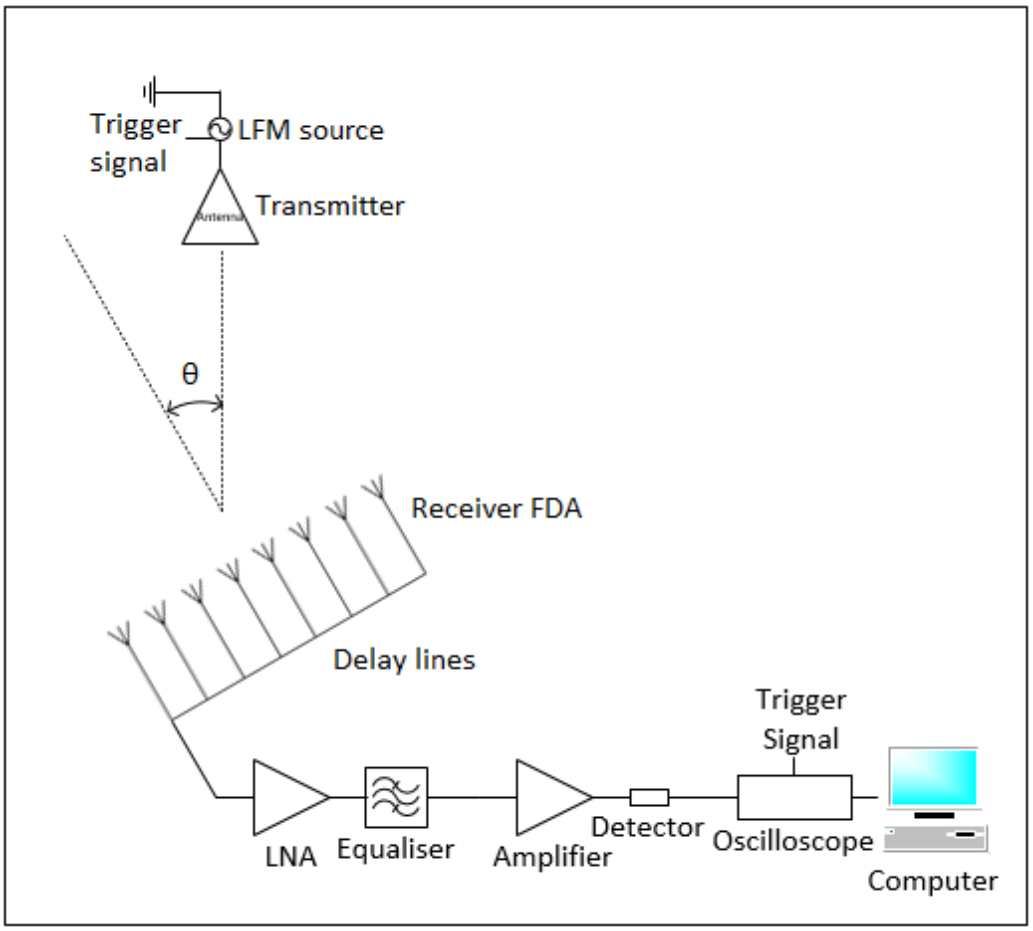

Figure 4.1: Sketch of the setup in the first experiment

Manufacturer codes of the elements in the transmitter and receiver chains are listed here with their basic features:

- Transmitter source: HMC587 with 0-5 dBm output power between 5-10 GHz
- Transmitter antenna for the first and the second experiment: Aselsan GAH4012 horn
- Transmitter antenna for the third experiment: Custom vivaldi antenna
- Receiver array: FDA with inter-element delay of 0.51 ns
- Magic Tee: Omni Spectra FSC16179 operates in 2-18 GHz
- LNA: TriQuint TGA2513 with 17 dB gain between 2-23 GHz

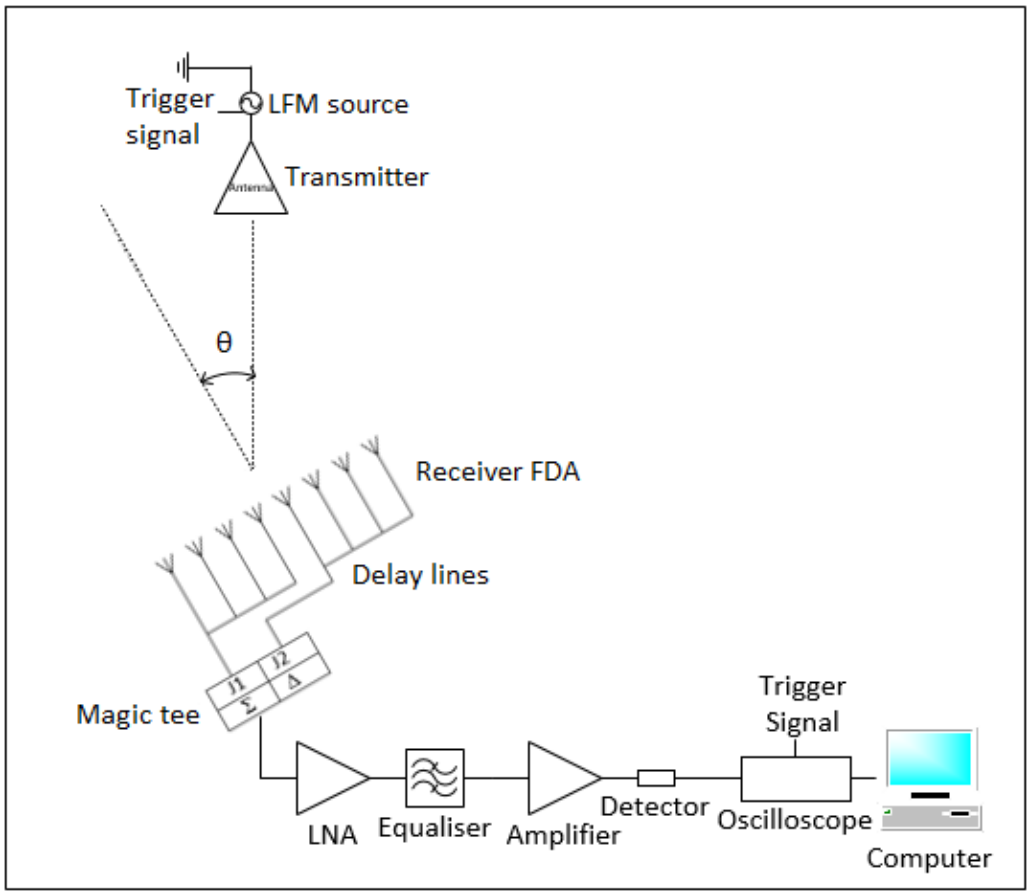

Figure 4.2: Sketch of the setup in the second experiment

- Equalizer: EQ2P5
- Power amplifier: Avantek AFT-18665-10F with 32.5 dB gain between 6-18 GHz
- Diode detector: Narda Miteq 4506 operates between 10 MHz - 18 GHz with ∓0.5 dB flatness
- Oscilloscope: DSO1022A with 200 MHz bandwidth

Main purpose of the first and the second experiment was to verify the basic ideas behind the DF methods with the one-way link. In one-way link, high SNR helped to prove the compatibility between the theory and calculations. Especially the timings and angle of arrivals should be accurately measured to verify the theory. In the monostatic scenario with a broad beamwidth, SNR is much lower and scenarios are

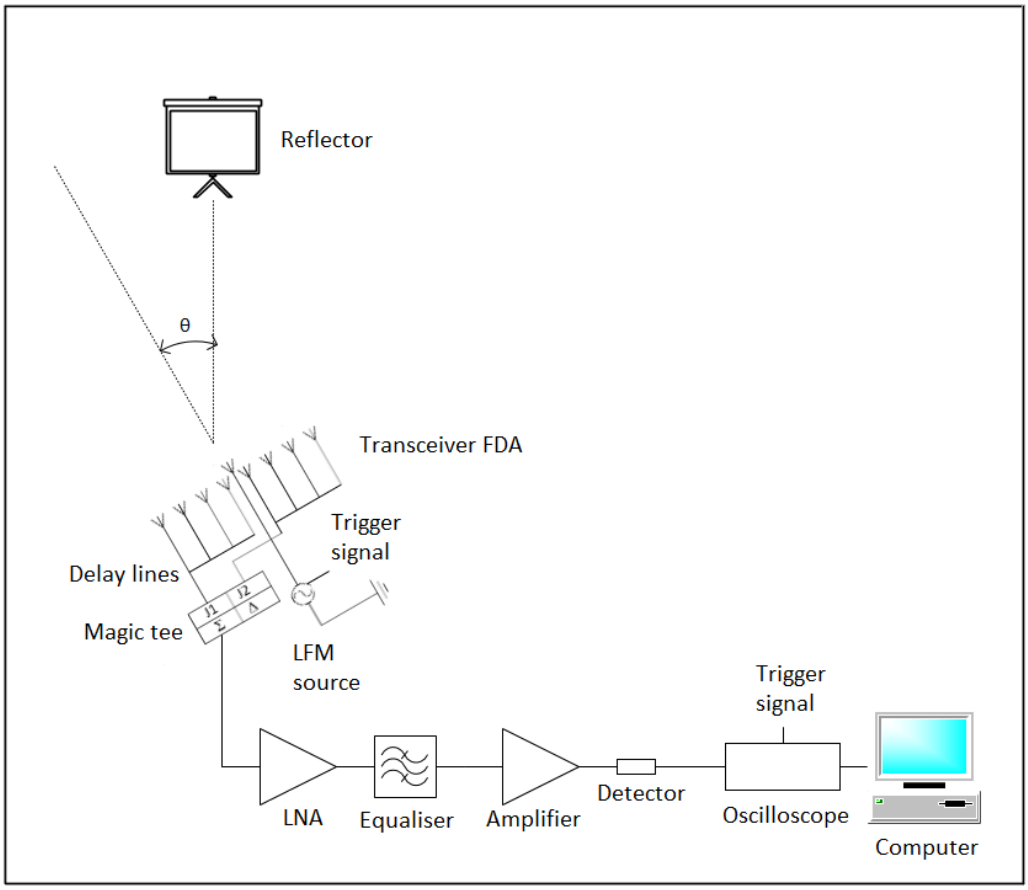

Figure 4.3: Sketch of the setup in the third experiment

more realistic.

Anechoic chamber of the Middle East Technical University was used in the experiments. In the experiments, receiver array was constructed on a rotatable platform so that the azimuthal angle can be accurately adjusted for each scenario. A motor controller was set to configure the platform to preferred direction. Algorithm of the controller was written in MATLAB and its accuracy is $\mp 0.036^o$ which is sufficient for our beamwidth. Inputs for the controller were entered from the MATLAB GUI.

An instrument control software (FDA GUI) was used in the experiments. It was written in Python by Çağrı ÇETİNTEPE. It helped to collect data from the oscilloscope and to arrange the tune voltage of the transmitter. Predistortion data for the VCO was embedded on this software. Bandwidth and center frequency can be directly adjusted. GUI for this software was also prepared by him to make it user-

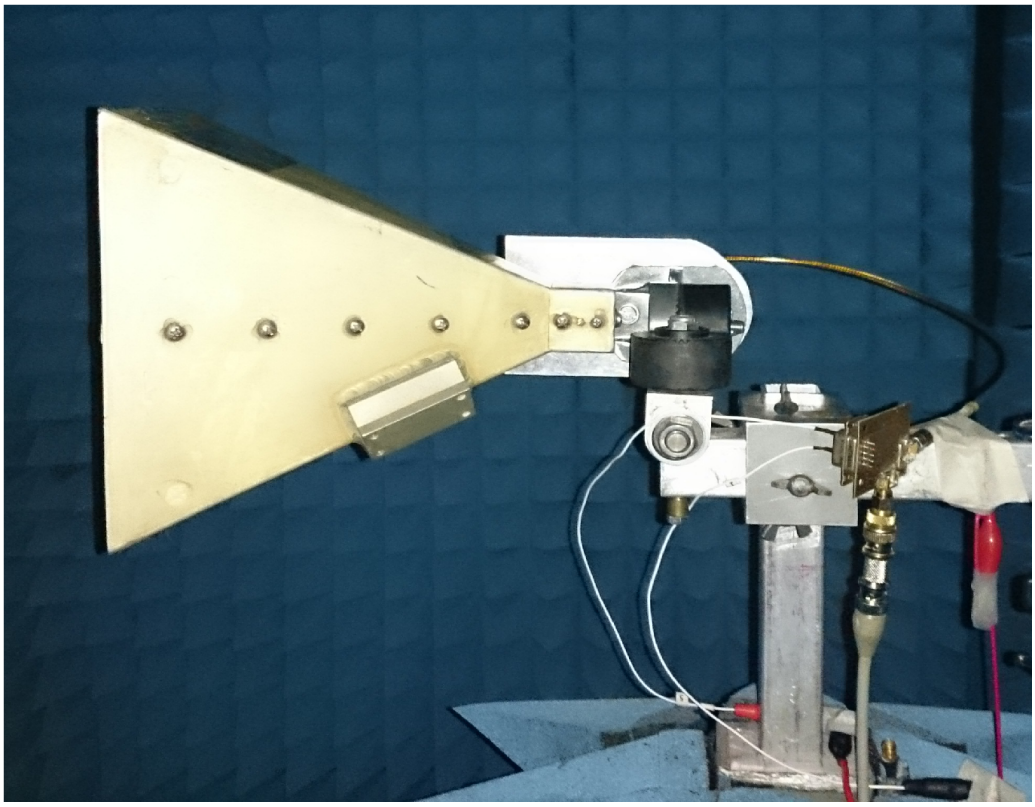

Figure 4.4: Photograph of the transmitter

friendly.

Transmitter source was a wideband VCO. In order to realize frequency modulation, sawtooth tune voltage was fed to VCO as it was given in Figure 3.5. Linearization for the tune voltage was done by the FDA GUI according to the center frequency and bandwidth. In the experiments, center frequency of 5.88 GHz was used with 0%, 5%, 10%, 15%, 20% and 25% bandwidths and 7.84 GHz was used with 0%, 5%, 10%, 15% bandwidths.

At 5.88 GHz and 7.84 GHz, receiving beam is directed towards the broadside. It is not compulsory to choose a center frequency that directs the beam to broadside at that frequency. But with these choices, azimuthal space can be scanned evenly.

Note that, for 0% bandwidth, array doesn't operate as LFM based FDA. It was used to measure the true position of the peak of the beam so that the residual error of the rotatable platform can be compensated.

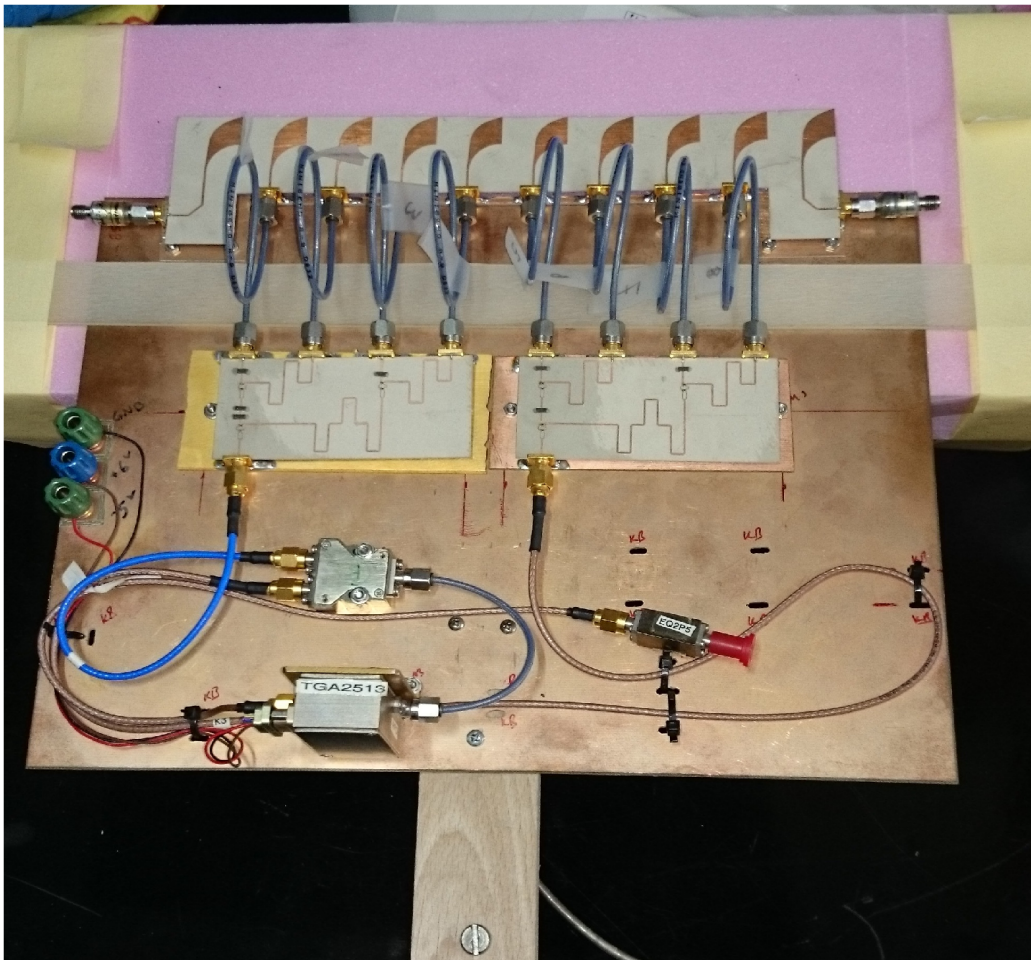

Figure 4.5: Photograph of the receiver array

Assume that array operates in a single frequency ω_o, (take $t = 0$). For $\theta = 0^o$ and $R_o = 0$, equation 3.8 becomes,

$$-\omega_o t_d = 2\pi\ell \tag{4.1}$$

For $\omega_o = 2\pi\ x\ 5.88\ x\ 10^9$ Hz and $t_d = 0.51$ ns, $\ell = -3$ holds. And for $\omega_o = 2\pi\ x\ 7.84\ x\ 10^9$ Hz and $t_d = 0.51$ ns, $\ell = -4$ holds. These calculations show that the chosen center frequencies direct the beam through the broadside.

Bandwidth selection determines the scan angle of LFM based FDA radar. For 0% bandwidth, there is no scanning. For other bandwidths, scan angles are calculated for each center frequency. Note that in equation 3.8, ω_o is not the center frequency but it

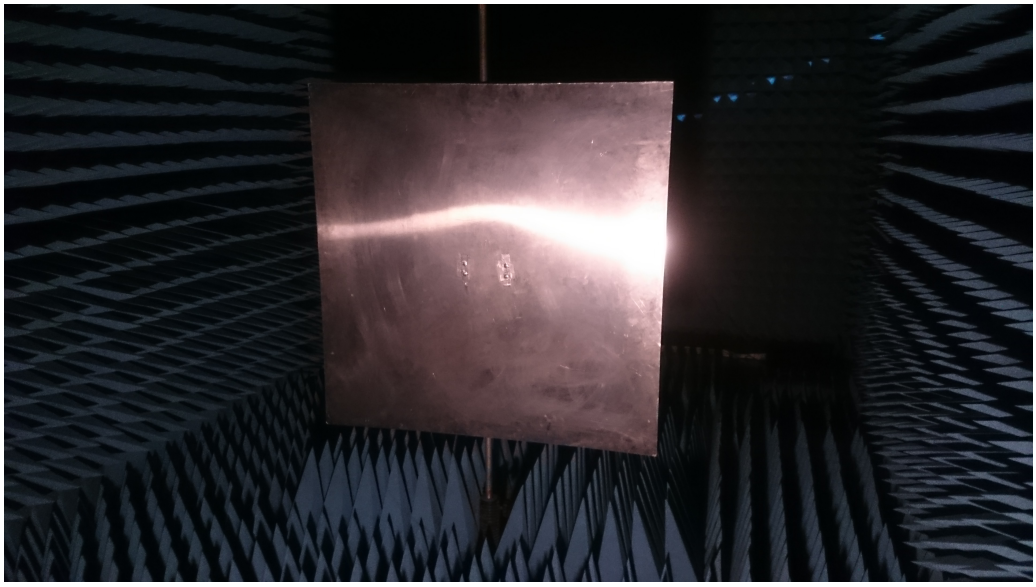

Figure 4.6: Photograph of the reflector

is the starting frequency and $(\omega_o + mt)$ expresses the instantaneous angular frequency.

For the center frequency of 5.88 GHz, calculations are done for 5%, 10%, 15%, 20% and 25% bandwidths. For 5% bandwidth, the lowest instantaneous angular frequency is $\omega_o + mt = 2\pi\ 5.88\ (1 - 2.5\%)\ 10^9 = 2\pi\ 5.733\ 10^9$ Hz and the highest instantaneous angular frequency is $\omega_o + mt = 2\pi\ 5.88\ (1 + 2.5\%)\ 10^9 = 2\pi\ 6.027\ 10^9$ Hz. For $R_o = 0$ and $t_d = 0.51$ ns at the lowest angular frequency, $\theta = -9.174^o$ is calculated from equation 3.8. And for the highest angular frequency, $\theta = 8.446^o$ is calculated. Note that in the lowest and highest frequencies, look angles are not symmetrical since the look angle and the frequency are not linearly proportional. However, they are not far away from each other either. For 5% bandwidth, scan angle is $9.174^o + 8.446^o = 17.62^o$.

For 10% bandwidth at 5.88 GHz, scan angle is 35.75^o; for 15% it is 55.00^o, for 20% it is 76.71^o and for 25% it is 103.96^o. This means that the backlobe of the array never becomes main lobe and each angle on space are scanned at most one time.

For 5% bandwidth at 7.84 GHz, scan angle is 17.63^o; for 10% bandwidth, scan angle is 35.75^o; for 15% it is 55.06^o.

Range resolution is calculated in [3] as in equation 4.2.

$$R_{res} \cong \frac{Nct_d}{4} \tag{4.2}$$

Note that, expression 4.2 is not valid for the 0% bandwidth case. For other cases, range resolution was approximately 0.3 m.

It is proposed in section 3.2.1 that the range should be found by the downconversion operation. However, range was not found in these experiments. It was taken as zero in the calculations. Range resolution was around 0.3 m. Therefore, it was fair to take the range that is more than 3 m as zero.

4.1.1 Encountered Difficulties in the Implementation Phase

In the implementation phase of the second and the third experiments, magic tee was used. Photograph of the magic tee is seen in Figure 4.7. It has 4 ports, namely J1, J2, sum ($\sum$) and difference (Δ) port. In the four port measurements of the magic tee, it was seen that the magic tee has phase imbalance between the measurements of J1 to $\sum$ port and J2 to $\sum$ port as it is seen on Figure 4.8. There is also phase deviation from 180^o between the measurements of J1 to Δ port and J2 to Δ port as it is seen on Figure 4.9.

It is shown in Figure 4.8 and 4.9 that the phase imbalances are not acceptable especially as the frequency goes higher. They are linearly increasing with the frequency. This means that there is a true time delay imbalance between the ports. This delay difference is calculated as approximately 7.5 ps.

In order to compensate the delay difference between the ports J1 and J2, a PCB was manufactured. It simply includes two delay lines as in Figure 4.7. It is connected to the input ports of the magic tee. After this operation, phase imbalance of the total system was measured for the $\sum$ port as in Figure 4.10. Phase imbalance for the Δ port was also measured as in Figure 4.11. Figure4.10 and 4.11 show that the phase imbalance was compensated by the delay lines. There are still some imbalances; however, these imbalances don't have linear relation with the frequency. Therefore, it is not possible to further compensate them. In addition, they were acceptable in the

Figure 4.7: Photograph of the magic tee

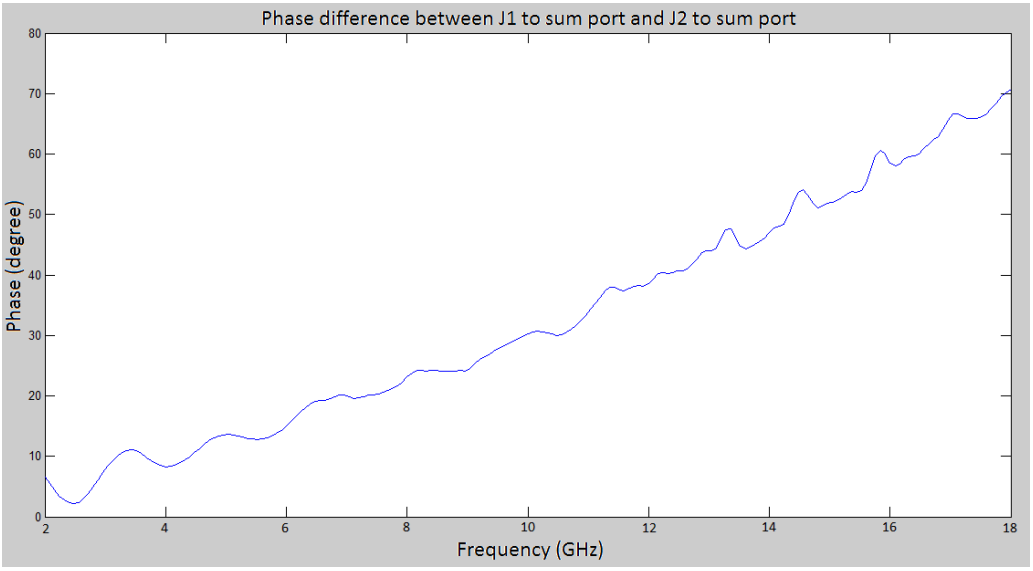

Figure 4.8: Phase imbalance between the measurements of J1 to $\sum$ port and J2 to $\sum$ port

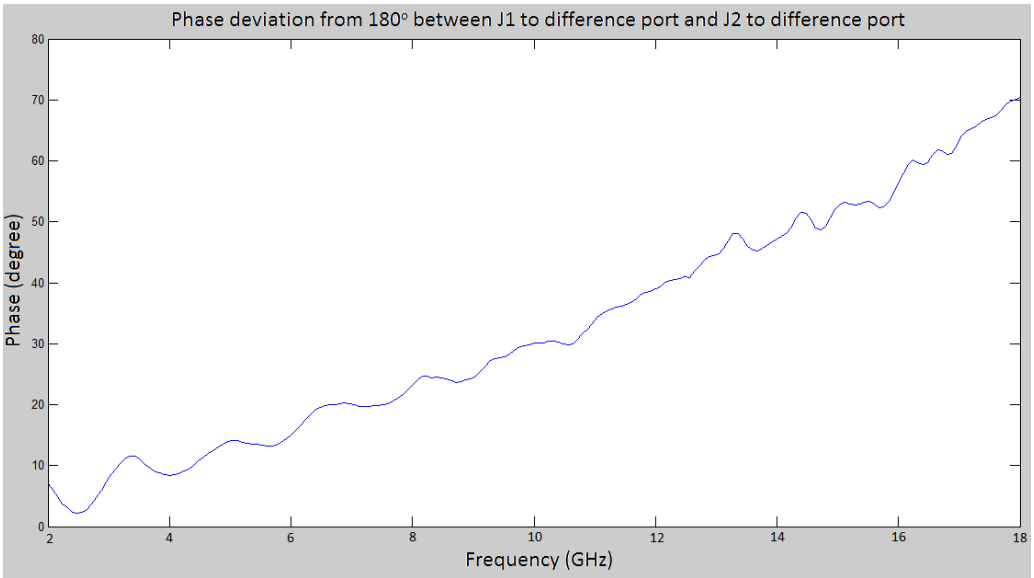

Figure 4.9: Phase deviation from 180^o between the measurements of J1 to Δ port and J2 to Δ port

frequency band of the experiments.

After this compensation, magic tee was used in the second and the third experiment with the compensation delay lines.

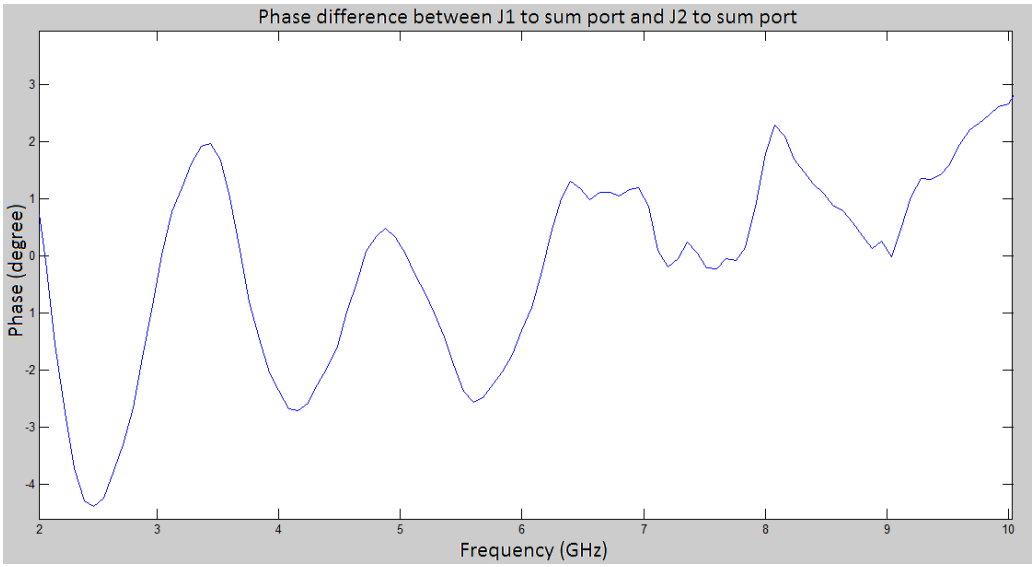

Figure 4.10: Phase imbalance between the measurements of J1 to $\sum$ port and J2 to $\sum$ port after the compensation

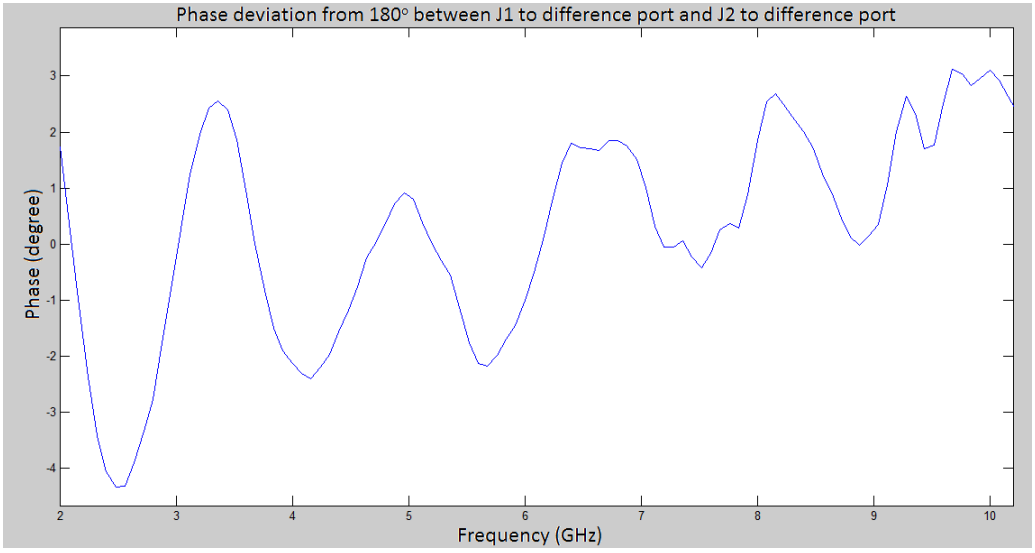

Figure 4.11: Phase deviation from 180^o between the measurements of J1 to Δ port and J2 to Δ port after the compensation

4.2 Results of the Experiments

In this section, experiments up to 5 m measurements are briefly summarized. Important inferences are made. Minimum range for these experiments was 3 m. Since 3 m is not far enough, the look-angle seen from the one end of the array is not approximately equal to the look-angle seen from the other end of the array. But this doesn't bring too much error. For the worst case with 3 m range and $\theta = 45^o$ look-angle, it is calculated that the absolute error originated from this fact is less than 0.02^o.

4.2.1 Results of the First Experiment

As it is said in the previous section, first experiment was an observation of the LFM based FDA waveforms and timings. In this experiment, setup that was described in Figure 4.1 was used. The parameters that are used in the scenarios are given with the measurement results for the pulse-width and look-angle. These results are also compared with the calculations.

4.2.1.1 Scenario 1

For the center frequency of 5.88 GHz, 25% bandwidth and $\theta = 0^o$ (directly looking towards each other), received signal was obtained as in Figure 4.12.

Note that for the repeated FM periods, repeated peaks were obtained. Here, FM period gives the scan rate. Scan period was 10 ms for these experiments which makes the scan rate 100 Hz. If this rate is increased, scanning can be done much faster. However, SNR for one pulse would be lower since the dwell time would be lower. Optimum solution depends on the target type. If the target is maneuvering and fast, high scan rates can be used. In order not to lower the total SNR for the low speed targets in this case, pulse integration should also be done.

Sidelobe level was measured as 16.3 dBc which is expected since the 13.2 dBc is the standard value for the uniform arrays. The little difference may be originated from

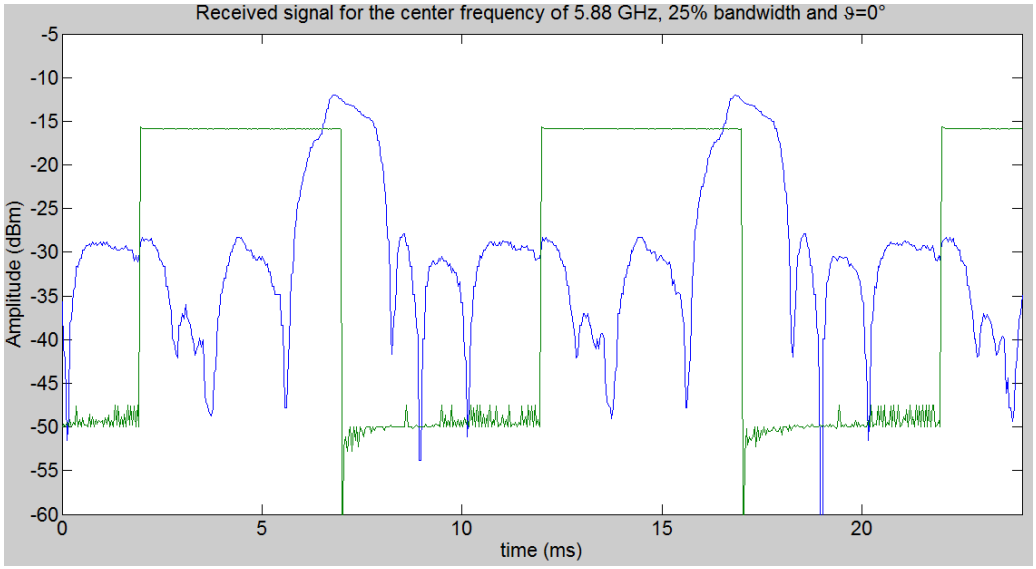

Figure 4.12: Received signal for the center frequency of 5.88 GHz, 25% bandwidth and $\theta = 0^o$ for the first experiment

the losses of the feedlines.

In order to decrease the sidelobe level, Taylor illumination can be used which was proposed in subsection 3.2.4. Decreasing the sidelobes decreases the false alarm rate, however, also decreases the gain. Therefore, one should find an optimum solution for the antenna design according to this fact.

Arrival instant of the peak of the pulse was 4.83 ms with reference to rising edge of the trigger signal in this scenario. Using the time of arrival data in equation 3.8 for the zero range, it is calculated that the look-angle is approximately -1.7^o which is very close to the angle that is arranged by the MATLAB GUI.

Note that the rising edge of the trigger signal corresponds to the starting point of the FM and falling edge of the trigger signal corresponds to the center frequency of the bandwidth. Since the center frequency was chosen as to point the boresight for the ranges close to zero, peak of the pulse in Figure 4.12 is close to the falling edge of the trigger signal. Little difference was originated from the characteristics of the diode detector.

Pulse-width is given in [3] as in equation 4.3.

$$\Delta t_{null-to-null} \cong \frac{2}{N\Delta f} \tag{4.3}$$

According to equation 4.3, null-to-null pulse-width is calculated for $N = 8$ and $\Delta f \cong 75$ Hz approximately as 3.33 ms while it was measured as 2.56 ms in this scenario. It can be seen that the results are close to each other. It was expected to have error in the null-to-null measurements due to noise level.

4.2.1.2 Scenario 2

In this scenario, same frequency and bandwidth were chosen (at 5.88 GHz, 25% bandwidth) for $\theta = 30^o$ and received signal was obtained as in Figure 4.13.

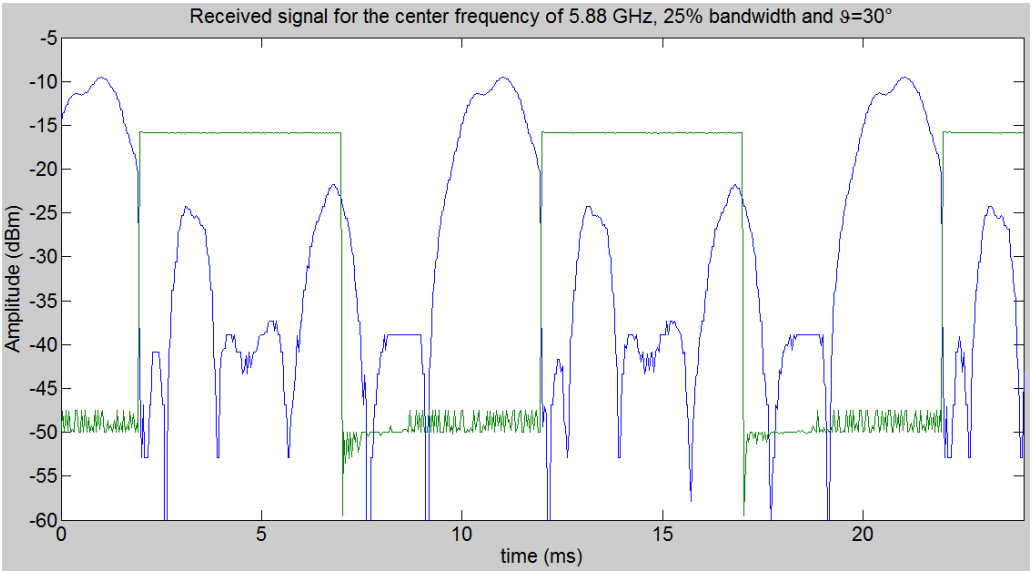

Figure 4.13: Received signal for the center frequency of 5.88 GHz, 25% bandwidth and $\theta = 30^o$ for the first experiment

Sidelobe level was measured as 12.2 dBc in this case. Frequency content of the main beam and the biggest sidelobe are different with respect to those of scenario 1. Different sidelobe level with respect to that of scenario 1 may be originated here because of the frequency response of the beam-former.

Scanning is done through the negative values to positive values of θ. Therefore, arrival time of the peak of the pulse should be late with respect to that of scenario 1. It

was measured as 9.04 ms with reference to rising edge of the trigger signal for this scenario.

Look-angle was calculated approximately as 34.0^o which is close to the angle that is arranged by the MATLAB GUI.

Null-to-null pulse-width couldn't be measured in this scenario since the pulse was truncated. It overlapped with the finishing instant of the FM. Beamwidth is too wide for this azimuthal angle. If one will implement LFM based FDA radar, antenna gain should be increased. Since these experiments are just aimed to prove the basic theory, this is ignored.

4.2.1.3 Scenario 3

In this scenario, center frequency was chosen as 7.84 GHz, and the bandwidth was 15%. For $\theta = 0^o$ (directly looking towards each other), received signal was obtained as in Figure 4.14.

Note that the center frequency was different than the previous scenarios. However, it was calculated that this frequency also corresponds to boresight for this setup.

Bandwidth is also different in this scenario. Note that it is not the instantaneous bandwidth that is referred here. It is the total bandwidth that is used. At an instant, array is filled with a part of the bandwidth and radiation occurs for this part of the bandwidth at that instant. This is the instantaneous bandwidth. Another bandwidth definition is in the calculations of the range resolution. Bandwidth that the target is exposed is used in these calculations, which is neither the total nor the instantaneous bandwidth.

Sidelobe level in this measurement was 16.1 dBc which is close to that of scenario 1.

Look-angle was found in this experiment approximately as 0.4^o which is very close to the angle that is arranged by the MATLAB GUI.

Null-to-null pulse-width is calculated for $\Delta f \cong 60\ Hz$ using equation 4.3 approximately as 4.17 ms while it was measured as 3.40 ms in this scenario.

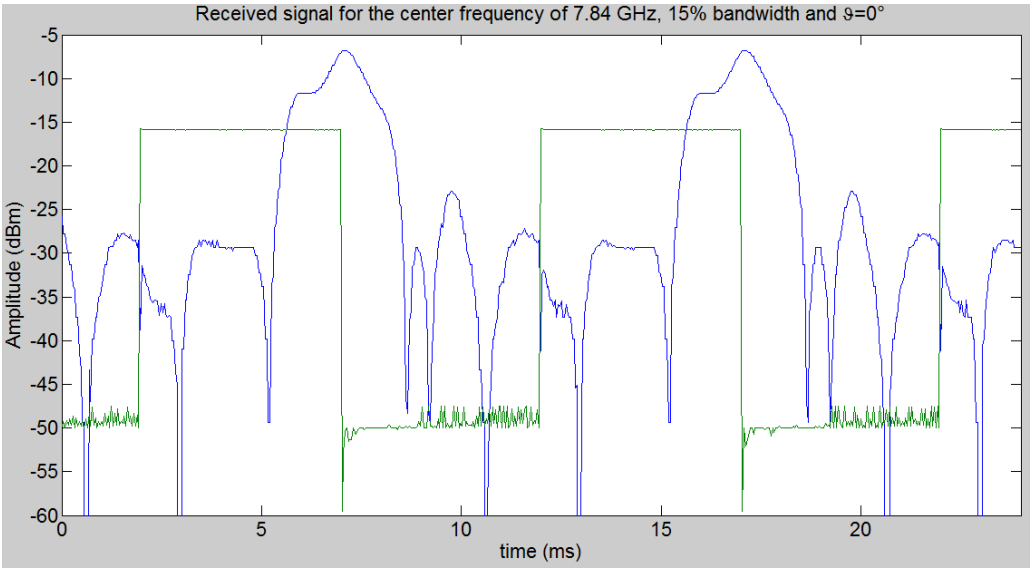

Figure 4.14: Received signal for the center frequency of 7.84 GHz, 15% bandwidth and $\theta = 0^o$ for the first experiment

Mismatch in the pulse-width is due to noise. However, since the SNR was high in the beam direction measurement, result is agreed with the calculation.

4.2.1.4 Scenario 4

For the same center frequency and bandwidth with the scenario 3, measurement was taken for $\theta = -15^o$. Received signal was obtained in this case as in Figure 4.15.

It was said that the center frequency corresponds to boresight for the look-angle for these experiments. Since $\theta = -15^o$ in this scenario, pulse comes before the falling edge of the trigger signal which corresponds to center frequency.

Look-angle was found approximately as -14.9^o which is close to the angle that is arranged by the MATLAB GUI.

Null-to-null pulse-width was measured approximately as 3.68 ms. Note that the pulse-width has certain relation with the look-angle and the instantaneous center frequency. Since equation 4.3 is an approximation, this relation is not included in the formula. In this scenario, physical aperture was appearing to be small in the direction of look-angle with respect to scenario 3. In addition, instantaneous center frequency

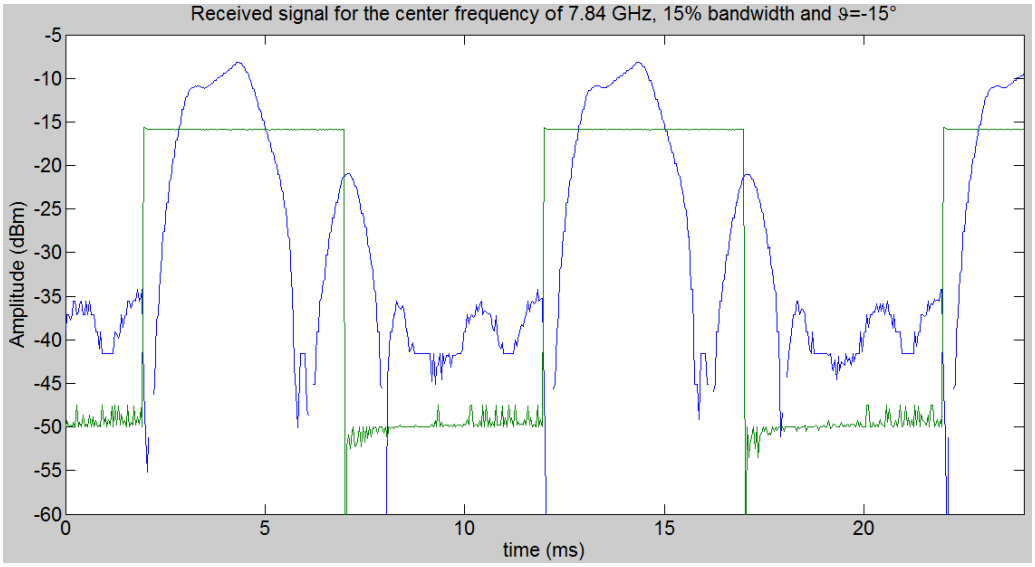

Figure 4.15: Received signal for the center frequency of 7.84 GHz, 15% bandwidth and $\theta = -15^o$ for the first experiment

at the instant of pulse formation was lower than the previous scenario. Because of these reasons, it is expected to have wider pulse-width with respect to the scenario 3.

4.2.2 Results of the Second Experiment

After it was seen that the measurements are agreed with the expectations in the first experiment, second experiment was prepared to demonstrate DF. In this experiment, magic tee was used for this reason. Sketch of the setup was given in Figure 4.2. Results of some measurements for the sum and difference patterns are given with the relevant parameters and the expectations for the pulse-width and angle of arrival.

4.2.2.1 Scenario 1

For the center frequency of 5.88 GHz, 25% bandwidth and $\theta = 0^o$ (directly looking towards each other), received signal for the sum and difference patterns were obtained as in Figure 4.16 and 4.17.

This scenario for the sum channel is similar with the scenario 1 of the first experiment.

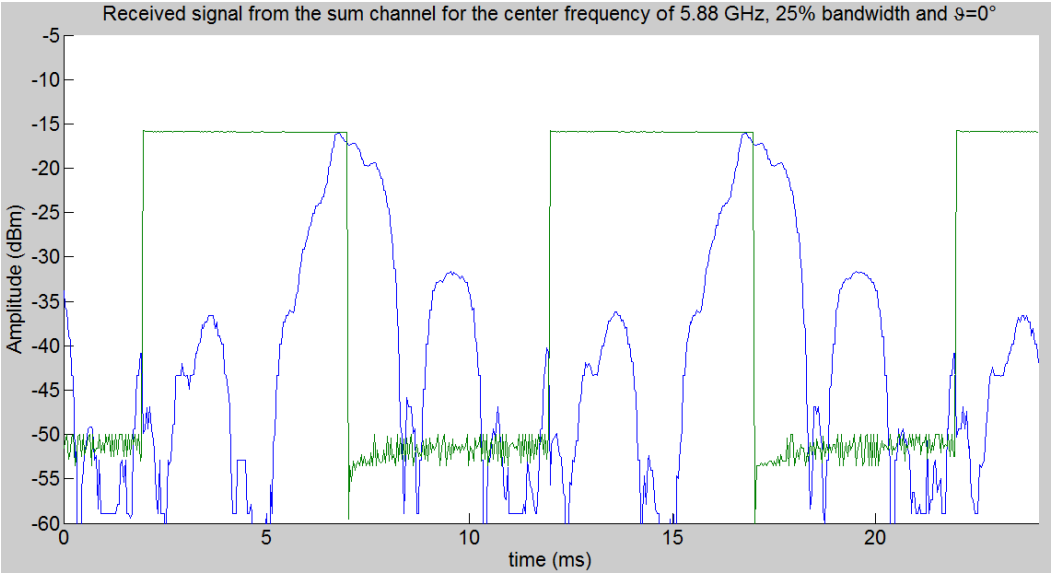

Figure 4.16: Received signal from the sum channel for the center frequency of 5.88 GHz, 25% bandwidth and $\theta = 0^o$ for the second experiment

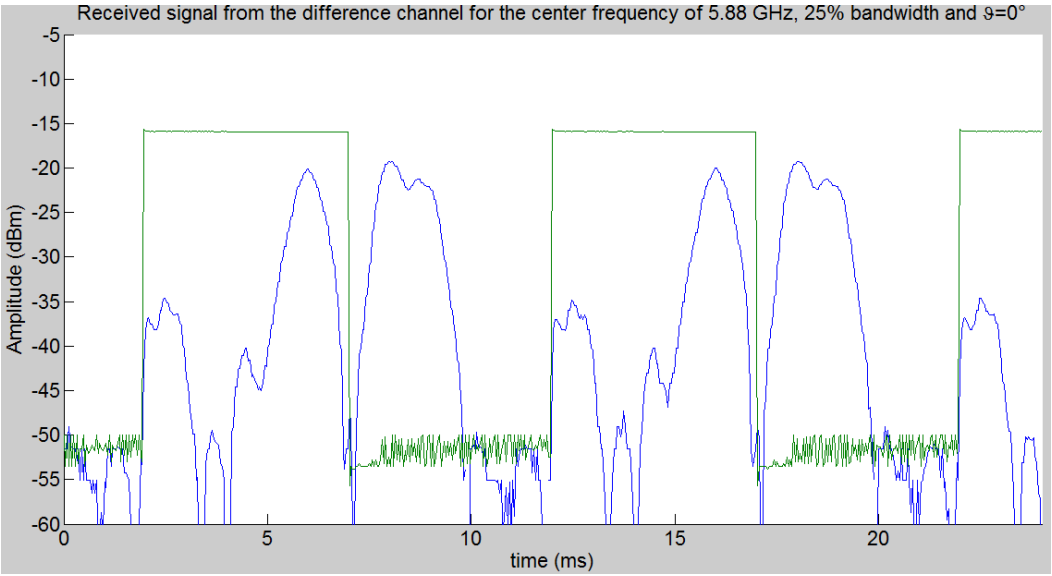

Figure 4.17: Received signal from the difference channel for the center frequency of 5.88 GHz, 25% bandwidth and $\theta = 0^o$ for the second experiment

Peak level is 4 dB lower in this case which is originated from the losses in the magic tee.

Sidelobe level was measured as 15.7 dBc which is close to that of the first scenario of

the first experiment.

According to equation 4.3, null-to-null pulse-width is calculated for the sum pattern as 3.33 ms which is agreed with the measurement, 3.24 ms.

In order to find the angle of arrival, difference pattern was divided by sum pattern and the DF algorithm was used. In the algorithm, equation 3.8 is solved. Note that the time data comes from this measurement with the null detection and range was taken as zero. The algorithm simply looks for the minima in the error signal pattern around the arrival instant of the peak of the pulse in the sum channel.

It is found from the algorithm that the angle of arrival was $\theta = -0.1^o$ which is close to the accuracy of the MATLAB GUI. DF algorithm will also be given in the appendix.

4.2.2.2 Scenario 2

For the center frequency of 5.88 GHz, measurement with the different bandwidth is given here. 15% bandwidth was used for the look angle of $\theta = -20^o$. Received signal for the sum and difference patterns were obtained as in Figure 4.18 and 4.19.

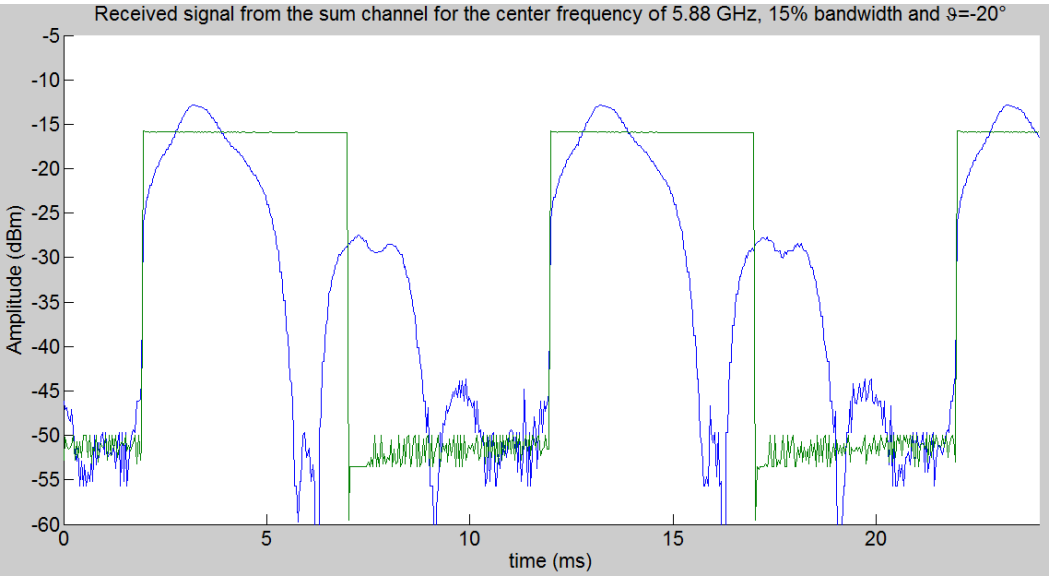

Figure 4.18: Received signal from the sum channel for the center frequency of 5.88 GHz, 15% bandwidth and $\theta = -20^o$ for the second experiment

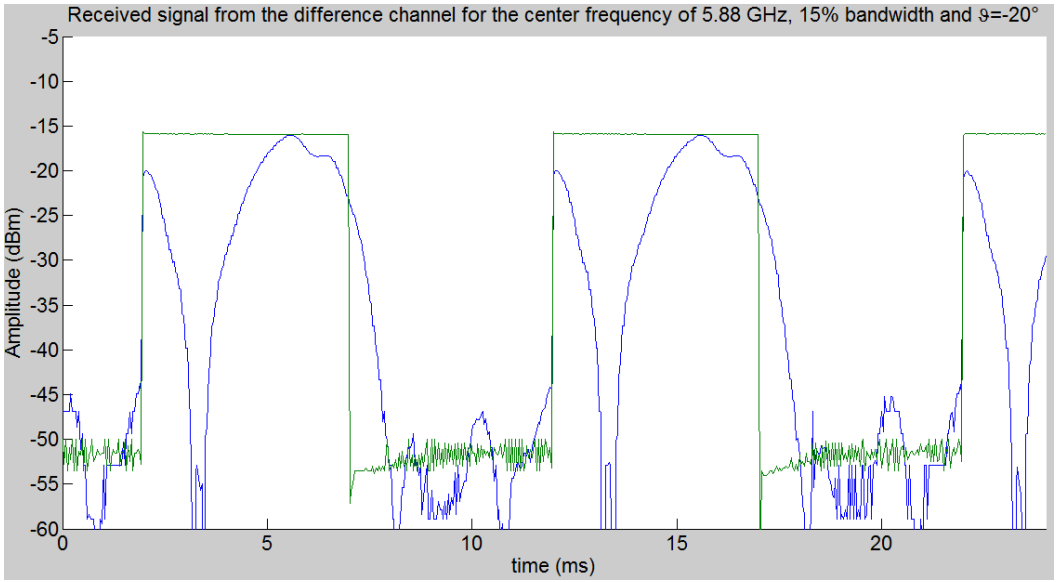

Figure 4.19: Received signal from the difference channel for the center frequency of 5.88 GHz, 15% bandwidth and $\theta = -20^o$ for the second experiment

Sidelobe is close to the previous scenario. 14.9 dBc was measured in this case.

Peak of the sum pulse is formed at 1.22 ms with reference to rising edge of the trigger signal. It is on the left side of the falling edge of the trigger signal since θ is negative.

As it is seen on Figure 4.18, sum pulse was truncated, since it overlapped with the starting instant of the FM. Therefore, pulse-width measurement was not valid. As it was said, in order not to lose the signal, antenna gain should be increased.

Difference signal was also truncated. However, since the peak of the sum pulse and the null of the difference signal form at the same time, null is always seen as long as the peak of the sum pulse forms.

In the DF algorithm, equation 3.8 is solved and it is found that the angle of arrival was $\theta = -21.4^o$ which is very close to the angle that is arranged by the MATLAB GUI.

4.2.2.3 Scenario 3

Another scenario is given here for different center frequency. 7.84 GHz is used here with 15% bandwidth. Look-angle was $\theta = 15^o$ in this scenario. Received signal for

the sum and difference patterns were obtained as in Figure 4.20 and 4.21.

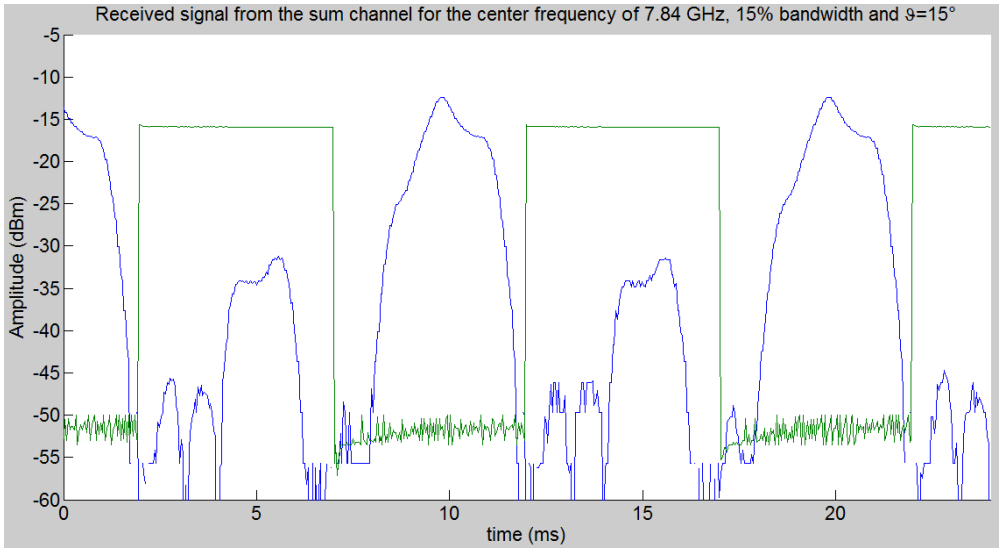

Figure 4.20: Received signal from the sum channel for the center frequency of 7.84 GHz, 15% bandwidth and $\theta = 15^o$ for the second experiment

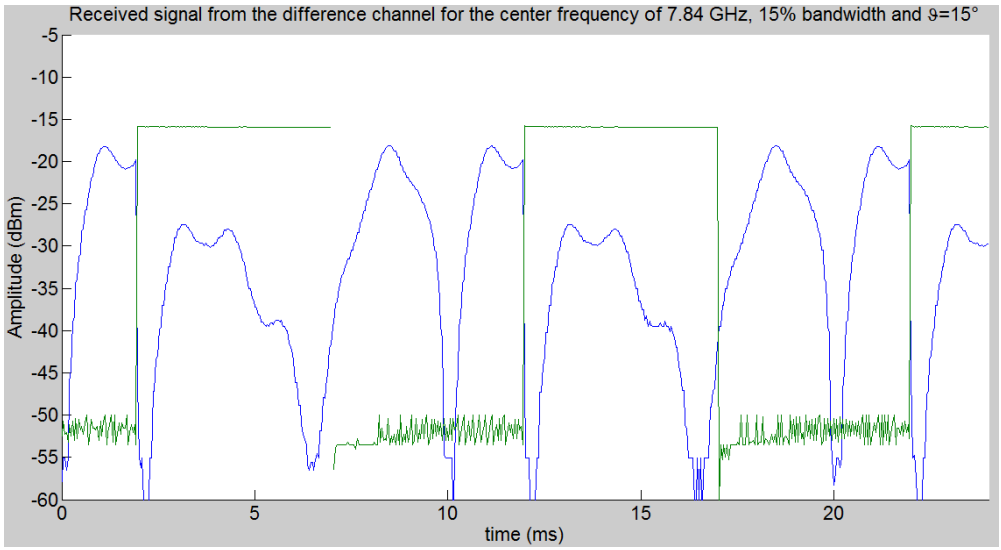

Figure 4.21: Received signal from the difference channel for the center frequency of 7.84 GHz, 15% bandwidth and $\theta = 15^o$ for the second experiment

In this scenario, sidelobe level for the difference pattern is high. However, since the detection was based on the sum pulse, sidelobes in the difference channel are not important. The reason of these sidelobes may be the frequency response of the beam-forming network.

Sum pulse comes after the falling edge of the trigger signal which is the consequence of the positive look-angle, θ.

Theoretical null-to-null pulse-width is calculated from equation 4.3 for $\Delta f \cong 60\ Hz$ as 3.69 ms which is close to the measurement, 3.80 ms. It is seen that the pulse of the difference channel was truncated since it overlapped with the finishing edge of the FM.

In the DF algorithm, equation 3.8 is solved and it is found that the angle of arrival was $\theta = 15.5^o$ which is very close to the angle that is arranged by the MATLAB GUI.

4.2.2.4 Scenario 4

Lastly, a scenario is given here to demonstrate the asymmetries on the pulse shapes. 5.88 GHz is used with 25% bandwidth. At the look-angle of $\theta = 25^o$, asymmetries can be easily seen. Received signal for the sum and difference patterns are given in Figure 4.22 and 4.23.

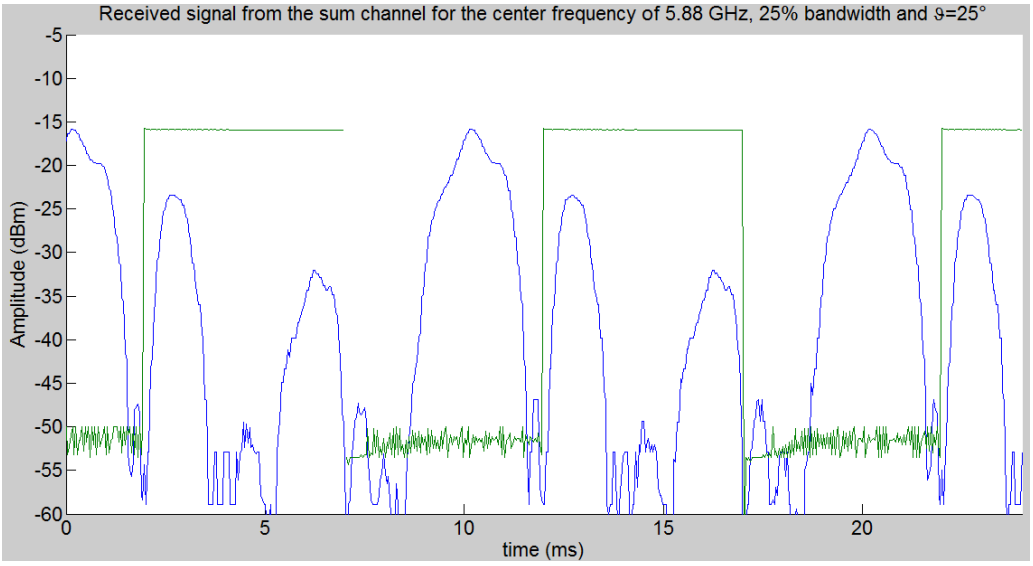

Figure 4.22: Received signal from the sum channel for the center frequency of 5.88 GHz, 25% bandwidth and $\theta = 25^o$ for the second experiment

In this scenario, there is a large sidelobe in the sum channel. It is far away from the real signal. It would not disturb the resolving of the two close targets. However, it

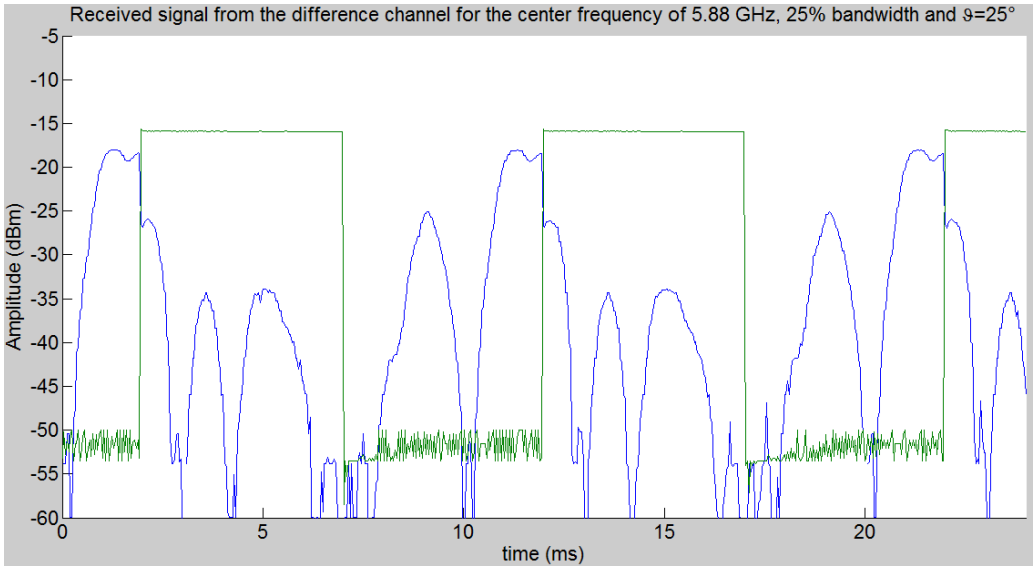

Figure 4.23: Received signal from the difference channel for the center frequency of 5.88 GHz, 25% bandwidth and $\theta = 25^o$ for the second experiment

may pass the threshold and create a false alarm. Therefore, it may be beneficial to use low sidelobe antenna for LFM based FDA radar design as it is also done in the conventional radars.

In this scenario null-to-null pulse-width was measured as 3.08 ms which is close to that in scenario 1.

It is said that the instantaneous center frequency and the aperture size on the direction of look-angle affects the pulse-width. In this scenario, both of them were different than those of scenario 1. However, pulse-widths are still close to each other since their effects cancel each other. Instantaneous center frequency was higher in the direction of look-angle in this scenario which increases the gain. And the aperture size on the direction of look-angle was small in this scenario which decreases the gain. Total effects make the pulse-widths close to each other.

This scenario also clearly demonstrated the asymmetries on the pulse shapes. Especially in Figure 4.23, it is obviously seen that the pulse from the difference channel has huge asymmetries between its wings.

By the DF algorithm, angle of arrival was found as $\theta = 26.1^o$.

4.2.2.5 Summary of the Second Experiment

In the DF measurements, parameters of the received pulse were measured for each scenario. Here, only four of them are presented. There were numerous scenarios and it is not possible to present all of them here. Measurements were taken by FDA GUI that was written by Çağrı ÇETİNTEPE which allows realizing multiple scenarios with one shot measurement.

In order to summarize the results quantitatively, a table is prepared for the center frequency of 5.88 GHz for 25% bandwidth, table 4.1. It is shown in the table that the results aligned with the expected values. $\mp 2^o$ direction accuracy was obtained with 15^o beamwidth in 70^o angular coverage.

Table 4.1: Results of the DF Experiment for LFM Based FDA at the Center Frequency of 5.88 GHz, 25% Bandwidth

Look-angle θ^o	Measured angle (degree)	|Biases + Errors| (degree)
35	36.5	1.5
30	30.9	0.9
25	26.1	1.1
20	21.8	1.8
15	15.8	0.8
10	10.1	0.1
5	4.4	0.6
0	-0.1	0.1
-5	-5.1	0.1
-10	-10.3	0.3
-15	-15.7	0.7
-20	-21.4	1.4
-25	-25.8	0.8
-30	-30.4	0.4
-35	-34.8	0.2

It is seen from the table that the addition of biases and errors increase as the receiver array strays from the boresight. Since SNR is high in this experiment, biases are dominant with respect to errors. However, it is also expected to have larger errors on the look-angles that are far away from the boresight. There are some reasons for this

fact. One of them is to have lower gain on the extreme angles. Another is the velocity of the beam rotation where the beam is faster on those angles. These two reasons decrease the SNR and decrease the chance to locate the null properly. Another fact is that the pulses become asymmetrical in those angles. Therefore, it is hard to locate target without the DF algorithm that is robust for the asymmetries. For this reason, it is beneficial to use pattern recognition improvement, as it is described in 3.2.4.

4.2.3 Results of the Third Experiment

Second experiment proved the basic idea behind the DF methods. After that, in order to realize more realistic situation, third experiment was conducted as a monostatic radar. In this experiment, setup that is described in Figure 4.3 was used. There were two cases in this experiment. One case was for approximately 3 m range and the other was for approximately 5 m. In order to observe the different pulses from different frequencies and bandwidths for two different ranges, 2 scenarios are chosen for short range and 2 scenarios are chosen for the long range for the demonstration. In these scenarios, $\theta = 20^o$ is observed for 5.88 GHz center frequency and 25% bandwidth and $\theta = -20^o$ is observed for 7.84 GHz center frequency and 15% bandwidth. Results of the measurements are given here with the expectations for the pulse-width and angle of arrival.

4.2.3.1 Scenario 1

For short range measurement at the center frequency of 5.88 GHz, 25% bandwidth and $\theta = 20^o$, received signals were found as in Figure 4.24 and 4.25 for the sum and difference patterns respectively.

Dominant sidelobe in the sum pattern seems to hide on the non-illuminated angles since the FM period is not large enough to cover those angles. If the target was closer to the broadside, the sidelobe would be apparent.

Null-to-null pulse-width was 3.56 ms which is matched with the expectation. Note that the main beam and sidelobe merged in some angles. Therefore, this measurement

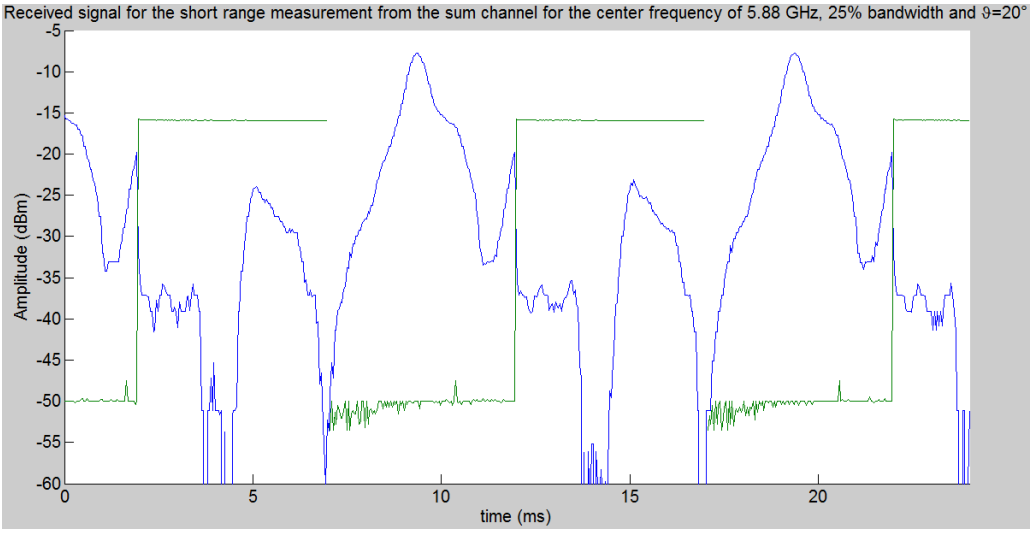

Figure 4.24: Received signal for the short range measurement from the sum channel for the center frequency of 5.88 GHz, 25% bandwidth and $\theta = 20^o$ for the third experiment

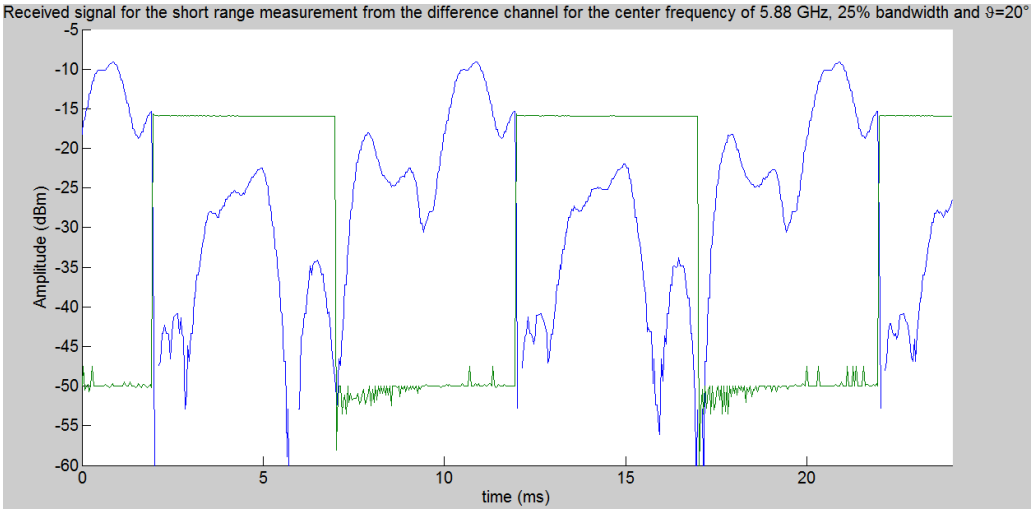

Figure 4.25: Received signal for the short range measurement from the difference channel for the center frequency of 5.88 GHz, 25% bandwidth and $\theta = 20^o$ for the third experiment

was not an exact width. Even so, it is useful data to compare with the expectations.

Difference pattern is seen in Figure 4.25 around the instant that the peak of the sum pulse formed. Null seems to be around the amplitude of -30 dBm. However, as it will be demonstrated later, noise level is below -40 dBm. The reason of this rise in the

amplitude of the null of the difference pattern is probably to have improper antenna weightings for this scenario.

Notice that the wings of the difference pattern are not symmetrical. The reasons of this are described in the preceded sections. This scenario is another proof for the theoretical assumptions.

DF algorithm was the same with the one that was used for the second experiment. According the outputs of the algorithm, angle of arrival was found as $\theta = 20.1^o$ which agrees with the angle that is arranged by the MATLAB GUI.

4.2.3.2 Scenario 2

For short range measurement at the center frequency of 7.84 GHz, 15% bandwidth at the look angle of $\theta = -20^o$, received signal for the sum and difference patterns were obtained as in Figure 4.26 and 4.27.

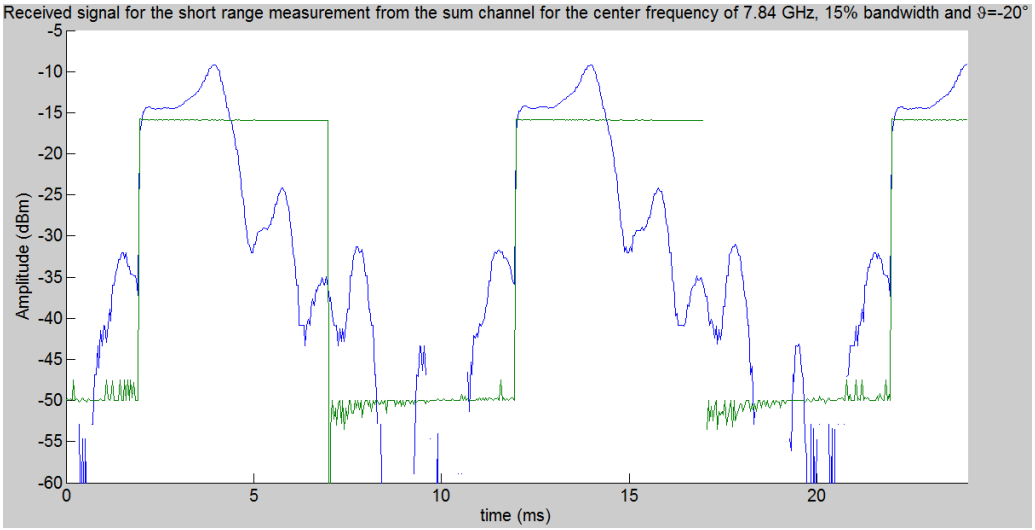

Figure 4.26: Received signal for the short range measurement from the sum channel for the center frequency of 7.84 GHz, 15% bandwidth and $\theta = -20^o$ for the third experiment

The signal level of the sum pattern is close to that of the previous scenario. However, signal shapes are not similar since the instantaneous frequency and look-angle are different. In the first scenario, the pulse was much sharper but there was a high

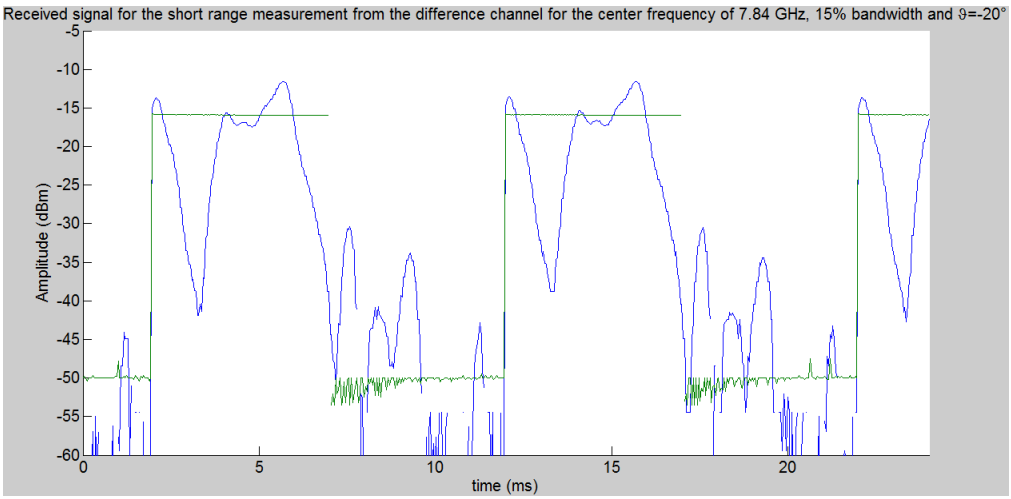

Figure 4.27: Received signal for the short range measurement from the difference channel for the center frequency of 7.84 GHz, 15% bandwidth and $\theta = -20^o$ for the third experiment

sidelobe. Here, pulse is flat but the sidelobe level is lower. Since the algorithm searches for a null in the difference pattern around the time instant that the peak of the sum pulse formed, it is not affected by the flatness.

Null of the difference pattern is more obvious in this scenario. It is seen that in the repetitive FM periods, level of the null is also changing since this level is close to the noise level.

Equation 3.8 is solved in the DF algorithm and angle of arrival was found as $\theta = -19.6^o$ which is close to the angle that is arranged by the MATLAB GUI. Difference was 0.4^o degree which is low with respect to the beamwidth which is approximately 11^o for this scenario.

4.2.3.3 Scenario 3

This scenario and the proceeded scenario are the long range scenarios. In these scenarios, range is around 5 m. In order to compare these scenarios with those of short range; same frequencies, bandwidths and look-angles are presented.

In this scenario, center frequency of 5.88 GHz is used with 25% bandwidth. Look-

angle was again $\theta = 20^o$ as in the first scenario. Received signal for the sum and difference patterns were found as in Figure 4.28 and 4.29.

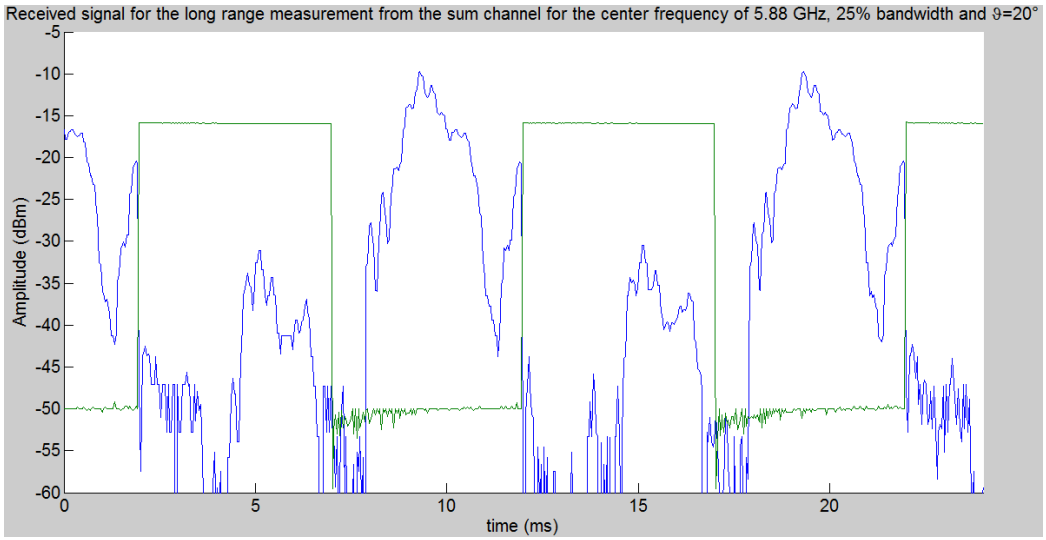

Figure 4.28: Received signal for the long range measurement from the sum channel for the center frequency of 5.88 GHz, 25% bandwidth and $\theta = 20^o$ for the third experiment

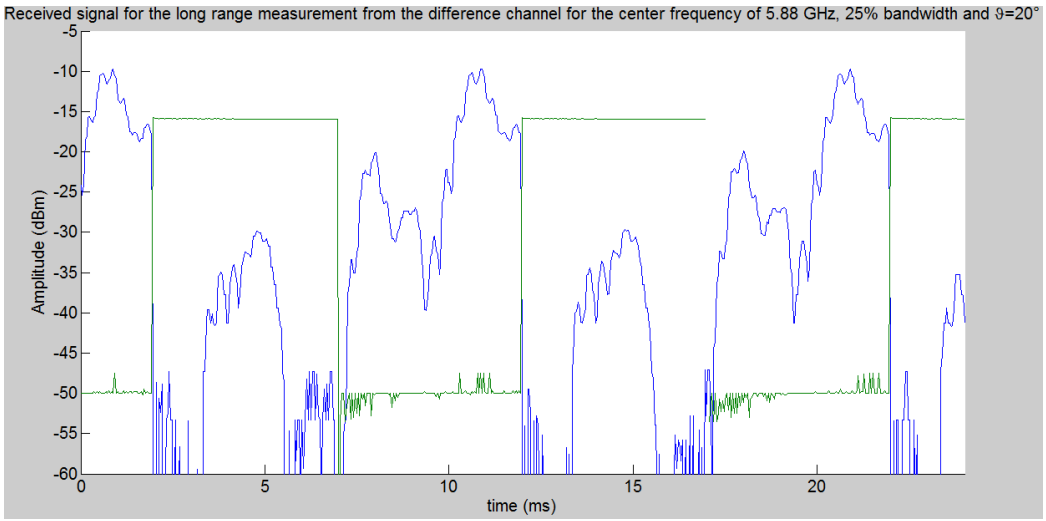

Figure 4.29: Received signal for the long range measurement from the difference channel for the center frequency of 5.88 GHz, 25% bandwidth and $\theta = 20^o$ for the third experiment

As it is seen in the figures, both sum and difference signals in the receiver are similar with those of scenario 1. Only significant difference is to have lower amplitudes

here. This proves the repeatability of the experiments. Noises on the signals are more obvious also in this scenario.

Null-to-null pulse-width can be measured approximately as 3.40 ms which is close to the theoretical value of 3.33 ms. It is also similar with the first scenario which was 3.56 ms.

Angle of arrival was found by the DF algorithm as $\theta = 19.5^o$ which can be considered as accurate measurement with respect to the beamwidth which is around 15^o for this scenario.

4.2.3.4 Scenario 4

Lastly, the scenario 2 is repeated for the long range and received signal for the sum and difference patterns were obtained respectively as in Figure 4.30 and 4.31.

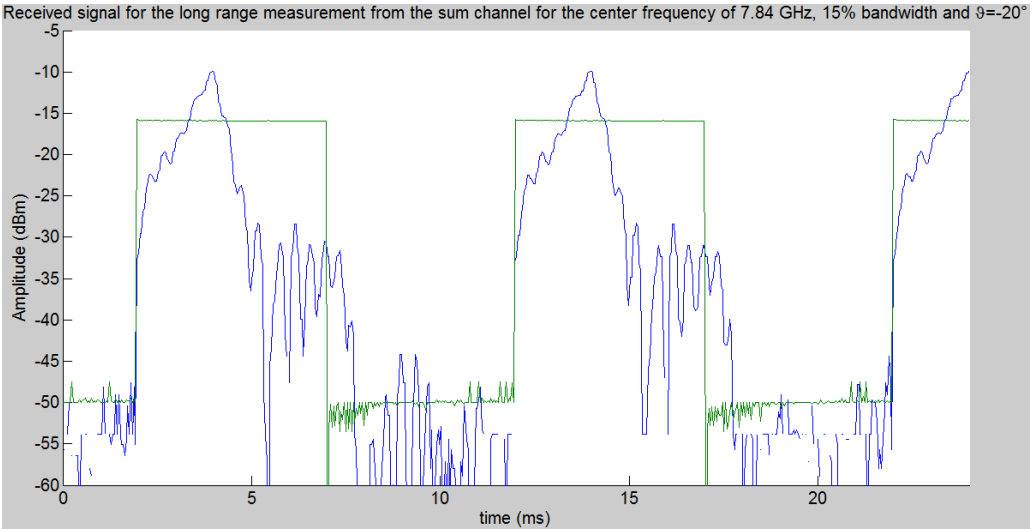

Figure 4.30: Received signal for the short range measurement from the sum channel for the center frequency of 7.84 GHz, 15% bandwidth and $\theta = -20^o$ for the third experiment

As it can be seen, signal shapes are similar to those of in the scenario 2. Here, both patterns are closer to the noise level. Dominance of the noise is obvious on some angles in this scenario.

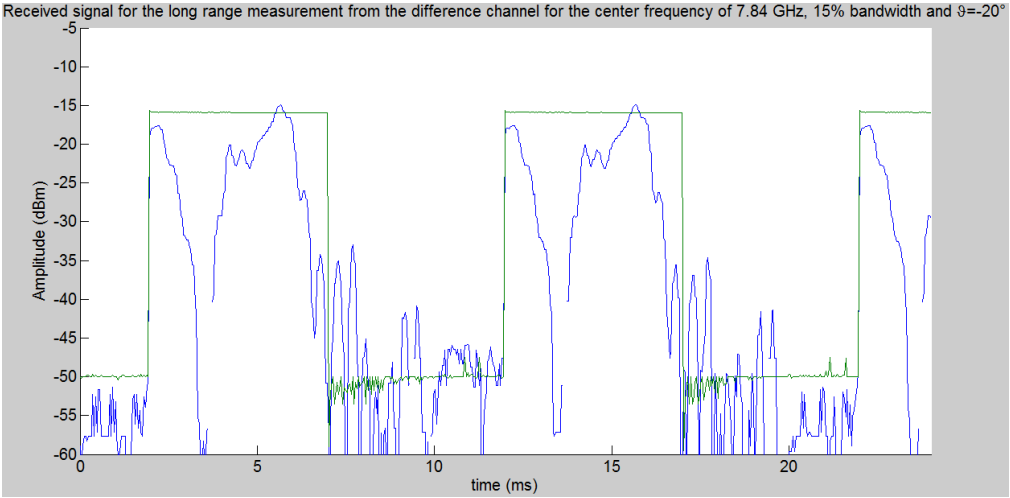

Figure 4.31: Received signal for the short range measurement from the difference channel for the center frequency of 7.84 GHz, 15% bandwidth and $\theta = -20^o$ for the third experiment

Angle of arrival was found as $\theta = -19.4^o$ by the DF algorithm. It is close to the angle that is arranged by the MATLAB GUI.

4.2.3.5 Summary of the Third Experiment

As an outcome of these measurements, it can be said that the first prototype of LFM based FDA radar was demonstrated successfully. To summarize the monostatic measurement results quantitatively, two tables are given for two different ranges and center frequency. Table 4.2 summarizes the results for the short range at the center frequency of 5.88 GHz for 25% bandwidth and table 4.3 is for long range at the center frequency of 7.84 GHz with 15% bandwidth. Note that at 7.84 GHz with 15% bandwidth, azimuthal coverage is approximately 55^o. Therefore, results are meaningless beyond $\theta = \mp 25^o$ at 7.84 GHz.

The tables demonstrate the capability of the LFM based FDA as radar. In some angles, there are slightly big misdirections since the DF algorithm was not sufficiently complex. Nevertheless, results are satisfactory for the poor SNR case. If the pattern recognition is done, as it is described in 3.2.4, it would have huge benefit.

Table 4.2: Results of the Monostatic DF Experiment for LFM Based FDA for the Short Range at the Center Frequency of 5.88 GHz, 25% Bandwidth

Look-angle θ^o	Measured angle (degree)	|Biases + Errors| (degree)
35	35.8	0.8
30	29.2	0.8
25	25.1	0.1
20	20.1	0.1
15	15.8	0.8
10	9.5	0.5
5	4.0	1.0
0	2.6	2.6
-5	-4.0	1.0
-10	-10.3	0.3
-15	-14.5	0.5
-20	-18.9	1.1
-25	-23.2	1.8
-30	-23.6	6.4
-35	-30.9	4.1

Table 4.3: Results of the Monostatic DF Experiment for LFM Based FDA for the Long Range at the Center Frequency of 7.84 GHz, 15% Bandwidth

Look-angle θ^o	Measured angle (degree)	|Biases + Errors| (degree)
25	22.7	2.3
20	18.9	1.1
15	14.5	0.5
10	9.7	0.3
5	5.1	0.1
0	0.9	0.9
-5	-3.8	1.2
-10	-8.6	1.4
-15	-15.2	0.2
-20	-19.4	0.6
-25	-25.8	0.8

4.2.4 Results of the Noise and Coupling Measurements

In order to find SNR in the DF experiments, noise and coupling measurements were done in the anechoic chamber within the same environment as in the experiments. These are shared in this subsection with their interpretations.

4.2.4.1 Receiver Noise

Receiver noise is measured when the transmitter is off. It is given in Figure 4.32 for the center frequency of 5.88 GHz and 25% bandwidth for the sum channel. This setting and the setting with 20% bandwidth have the highest noises in the measurements. These bandwidths are the largest bandwidths in the radar settings. Therefore, it is expected to have the highest noises at these settings in the measurements.

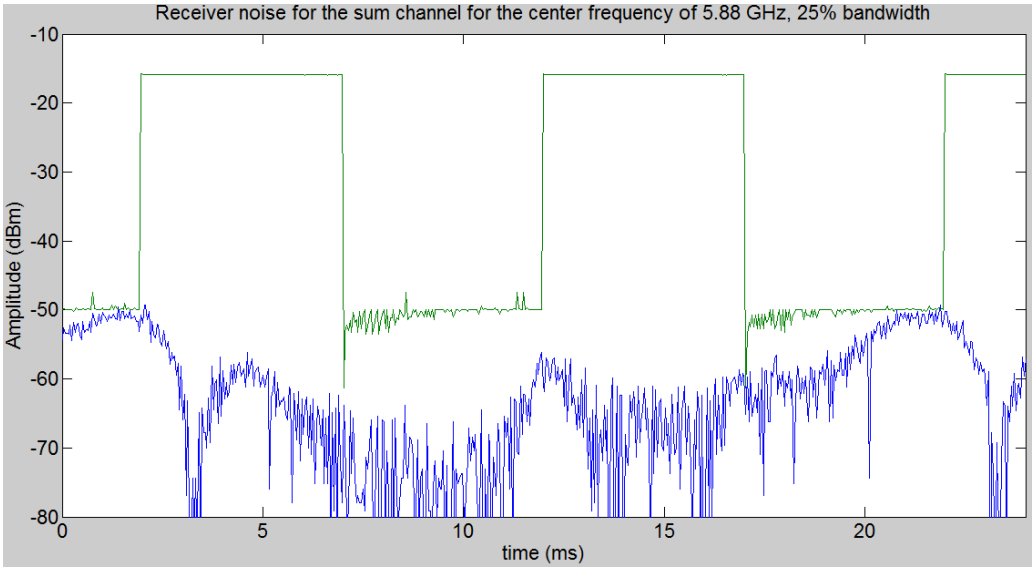

Figure 4.32: Receiver noise

The noise level of the difference channel is almost the same. Therefore, here, only the measurement for the sum channel is demonstrated. Also note that the target decision is made on the sum channel according to a threshold. Therefore, SNR of this channel is the critical one.

It is seen that the noise level is at maximum around -50 dBm which means that SNR was around 35 dB for the worst case in the second experiment which is good value for a radar receiver.

4.2.4.2 Noise and Coupling in the Receiver for the Monostatic Case

Spectrum that is apart from the useful signal for the monostatic case is shown in Figure 4.33 for the center frequency of 7.84 GHz and 15% bandwidth for the sum channel. This is actually the signal in the receiver without a target. At this frequency and bandwidth setting, noise and coupling were the highest. Again, the noise and coupling level of the difference channel was almost the same according to the measurements.

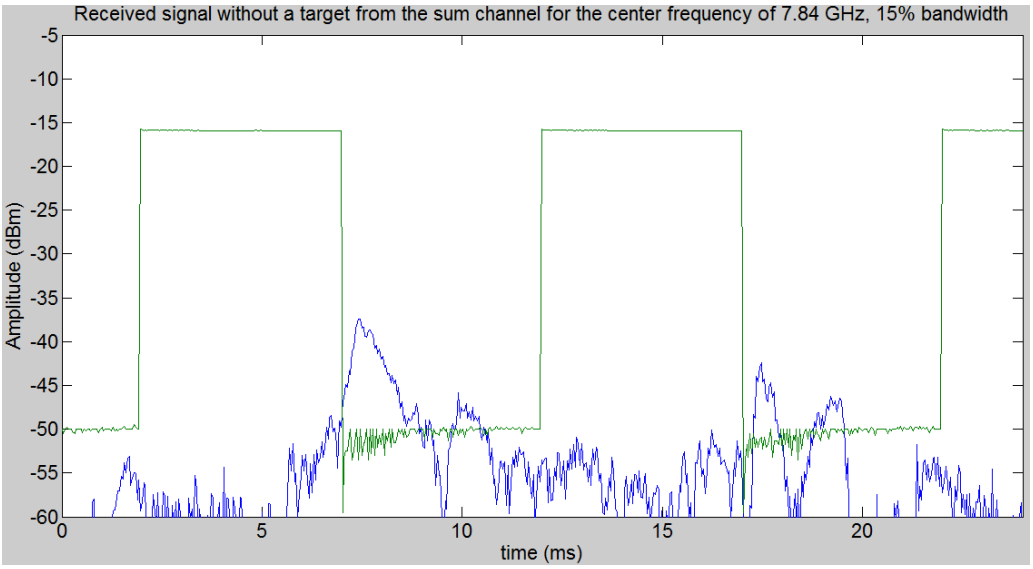

Figure 4.33: Signal in the receiver without a target

It is seen that the noise level is -37 dBm at its maximum. It is expected to have higher signal level in this case with respect to the noise measurement since the coupling raises the receiver floor. According to this measurement, SNR was around 27 dB for the worst case of the third experiment which is lower than that of the second experiment.

4.2.4.3 Relation between SNR and Direction Finding Accuracy

In order to see the relation between SNR and DF accuracy in the experiments, setup in Figure 4.2 which was used in the second experiment is constructed with an extra attenuator in the receiver and this experiment is compared with the results of the second experiment which was mentioned in subsection 4.2.2.

Results of the experiment with extra 17 dB attenuator is shown in the table 4.4. If it is compared with the results of the DF measurements in the second experiment, it can be seen that the results are poor with an extra attenuator.

Table 4.4: Results of the DF Experiment for LFM Based FDA at the Center Frequency of 5.88 GHz, 25% Bandwidth with an extra attenuator in the receiver

Look-angle θ^o	Measured angle (degree)	|Biases + Errors| (degree)
25	24.8	0.2
20	18.5	1.5
15	17.8	2.8
10	8.1	1.9
5	1.3	3.7
0	0.6	0.6
-5	-8.1	3.1
-10	-9.9	0.1
-15	-16.5	1.5
-20	-21.9	1.9
-25	-27.6	2.6

The average signal level is -26 dBm in this experiment where the average signal level in the second experiment was -15 dBm. The average of the addition of biases and errors of this experiment is calculated as 1.8^o where it was calculated for the second experiment approximately as 0.7^o. Since the SNR are high in both cases and misdirections are mostly originated from the biases, this experiments doesn't reveal the relation given in equation 4.4. However, it is seen that SNR has significant effect in the accuracy.

$$\sqrt{SNR} \propto 1/(absolute\ error) \tag{4.4}$$

CHAPTER 5

CONCLUSION AND FUTURE STUDIES

LFM based FDA is a promising technology and there are numerous advantages that can be adapted to radars. There are lots of studies that exploit the advantages of LFM based FDA for radar. This study is a part of them and DF technique for LFM based FDA radar is elaborated. This study is also important in regard to have experimental results. Compatible results with the theory are shown in the experiments.

In this study, DF methods are utilized with the antenna that illuminates the whole azimuthal coverage. However, it is possible to use directive antennas in the transmitter part. Azimuthal coverage can be divided into subsections and each section can be illuminated separately with a directive antenna. This can be another topic for the future study.

In the first and second experiment of this study, in order to prove the basic theory of the DF for LFM based FDA, one-way link was constructed. This helped to measure the basic parameters of the received pulse with high SNR. After that, monostatic case was demonstrated with a reflector. This experiment was the demonstration of the capability of LFM based FDA as radar in more realistic situation with poor SNR case. This was the first radar prototype of the LFM based FDA system. Furthermore, as a future study, one can try to resolve two targets in range and angle with this setup.

REFERENCES

[1] M. I. Skolnik, *Introduction to Radar Systems*, third edition ed. New York: McGraw-Hill, 2001.

[2] P. Antonik, M. C. Wicks, H. D. Griffiths, and C. J. Baker, "Frequency diverse array radars," in *2006 IEEE Conference on Radar*, April 2006, pp. 3 pp.–.

[3] T. Eker, "A conceptual evaluation of frequency diverse arrays and novel utilization of lfmcw," Ph.D. dissertation, 2011.

[4] C. Cetintepe, "Integration of rf mems technology with active components for radar applications," Ph.D. dissertation, 2015.

[5] B. R. Mahafza, *Introduction to Radar Analysis*. New York: CRC Press LLC, 1998.

[6] R. C. Johnson, *Antenna Engineering Handbook*, 3rd ed. New York: McGraw-Hill, 1993.

[7] A. V. Suchkov, "Frequency scanning monopulse slotted-waveguide antenna array," in *Trudy MAI*. Moscow Aviation Institute, 2016.

[8] A. A. Jerry, "Frequency-controlled scanning monopulse antenna," Mar. 18 1969, uS Patent 3,434,139. [Online]. Available: http://www.google.com.tr/patents/US3434139

[9] W. Kummer, A. Villeneuve, T. Fong, and F. Terrio, "Ultra-low sidelobes from time-modulated arrays," *IEEE Transactions on Antennas and Propagation*, vol. 11, no. 6, pp. 633–639, Nov 1963.

[10] M. Secmen, S. Demir, A. Hizal, and T. Eker, "Frequency diverse array antenna with periodic time modulated pattern in range and angle," in *2007 IEEE Radar Conference*, April 2007, pp. 427–430.

[11] M. Wicks and P. Antonik, "Frequency diverse array with independent modulation of frequency, amplitude, and phase," Jan. 15 2008, uS Patent 7,319,427. [Online]. Available: https://www.google.com/patents/US7319427

[12] J. Farooq, M. A. Temple, and M. A. Saville, "Application of frequency diverse arrays to synthetic aperture radar imaging," in *2007 International Conference on Electromagnetics in Advanced Applications*, Sept 2007, pp. 447–449.

[13] A. Abdalla, H. Abdalla, M. Ramadan, S. Mohamed, and T. Bin, "Overview of frequency diverse array in radar eccm applications," in *2017 International Conference on Communication, Control, Computing and Electronics Engineering (ICCCCEE)*, Jan 2017, pp. 1–9.

[14] Y. Wang, W.-Q. Wang, and H. Shao, "Frequency diverse array radar cramér-rao lower bounds for estimating direction, range, and velocity," in *International Journal of Antennas and Propagation*. Hindawi, 2014.

[15] W. Q. Wang and H. Shao, "Range-angle localization of targets by a double-pulse frequency diverse array radar," *IEEE Journal of Selected Topics in Signal Processing*, vol. 8, no. 1, pp. 106–114, Feb 2014.

[16] W. Q. Wang, "Subarray-based frequency diverse array radar for target range-angle estimation," *IEEE Transactions on Aerospace and Electronic Systems*, vol. 50, no. 4, pp. 3057–3067, October 2014.

[17] W. Q. Wang and H. C. So, "Transmit subaperturing for range and angle estimation in frequency diverse array radar," *IEEE Transactions on Signal Processing*, vol. 62, no. 8, pp. 2000–2011, April 2014.

[18] Z. Wang, W.-Q. Wang, and H. Shao, "Range-azimuth decouple beamforming for frequency diverse array with costas-sequence modulated frequency offsets," *EURASIP Journal on Advances in Signal Processing*, vol. 2016, no. 1, p. 124, Nov 2016. [Online]. Available: http://dx.doi.org/10.1186/s13634-016-0422-3

[19] K. Gao, W. Q. Wang, J. Cai, and J. Xiong, "Decoupled frequency diverse array range-angle dependent beampattern synthesis using non-linearly increasing frequency offsets," *IET Microwaves, Antennas Propagation*, vol. 10, no. 8, pp. 880–884, 2016.

[20] Y. Liu, "Range azimuth indication using a random frequency diverse array," in *2016 IEEE International Conference on Acoustics, Speech and Signal Processing (ICASSP)*, March 2016, pp. 3111–3115.

[21] R. Cetiner, S. Demir, and A. Hizal, "Range and angle measurement in a linear pulsed frequency diverse array radar," in *2017 IEEE Radar Conference (RadarConf)*, May 2017, pp. 0064–0067.

[22] A. Turhaner, S. Demir, and A. Hizal, "Monopulse direction finding for linear frequency modulation based frequency diverse array," in *2017 IEEE Radar Conference (RadarConf)*, May 2017, pp. 0089–0094.

[23] G. W. Stimson, *Introduction to Airbone Radar*. Mendham New Jersey: Scitech Publishing Inc., 1998.

[24] A. Wojtkiewicz, J. Misiurewicz, M. Nalecz, K. Jedrzejewski, and K. Kulpa, "Two-dimensional signal processing in fmcw radars," *Proc. XX KKTOiUE*, pp. 475–480, 1997.

[25] A. Meta, “Signal processing of fmcw synthetic aperture radar data,” Ph.D. dissertation, TU Delft, Delft University of Technology, 2006.

[26] D. E. Barrick, “Fm/cw radar signals and digital processing,” DTIC Document, Tech. Rep., 1973.

APPENDIX A

MATLAB CODE FOR THE DF ALGORITHM

```
clc
clear all
close all
f0=5.88; %GHz, 5.88 or 7.84
BW=25; %Percentage bandwidth

f=f0*1e9;
B=f*BW/100;

%Find the slope of the FM sweep
%0.01s is the period the sweep
m=B/0.01;

i=0;
Error=zeros(15,1);

%Convention for the angle in the measurement is different from
%the convention of the thesis
for Phi=55:5:125 %Increment is 5 degree, 90 is broadside
    i=i+1;

%Read the data
c_f0 = num2str(f0);
c_BW = num2str(BW);
c_Phi = num2str(Phi);
sdif = strcat('FDADif_Phi_',c_Phi,'_fc',c_f0,'_B',c_BW,'.csv');
```

```
ssum = strcat('FDASum_Phi_',c_Phi,'_fc',c_f0,'_B',c_BW,'.csv');
sdif = strcat('',sdif, '');
ssum = strcat('',ssum, '');
D = csvread(sdif,6,0);
S = csvread(ssum,6,0);

%Cut the signal for the one FM period
Dif_signal = D (51:301,2);
Sum_signal = S (51:301,2);

%Find the max of the signal
%(o/p of the peak detector is negative)
[V,I]=min(Sum_signal);

%Find the index of the min of the error signal
r=Dif_signal./Sum_signal;
[error,errorI]=min(r(I-min([(I-1) 10]):I+min([(249-I) 10])));
Min=errorI+I-min([(I-1) 10])-1;

%Find the time difference between the min of the error signal
%and the starting point of the FM sweep
%0.00004s is the time increment
TimeDif=(Min-1)*0.00004;

%FIND THE ANGLE

%Find the instantaneous frequency at the instant that
%the min of the error signal formed
fn=TimeDif*m+f-B/2;

%Solve the LFM based FDA equation

M=mod(2*fn*0.51e-9,2);
```

```
if M>1
    M=M-2;
end

Angle=asind(M*3e8/(2*0.025*fn));

%Find the error
Error(i,1)=abs((90-Phi)-Angle);
end

%Tabulate the outputs
T(:,1)=(35:-5:-35)';
T(:,2)=Error(:,1);
```